

## Neutrinos and Cosmic Rays Observed by IceCube

M. G. Aartsen<sup>b</sup>, M. Ackermann<sup>ba,\*</sup>, J. Adams<sup>p</sup>, J. A. Aguilar<sup>l</sup>, M. Ahlers<sup>ad</sup>,  
M. Ahrens<sup>ap</sup>, I. Al Samarai<sup>y</sup>, D. Altmann<sup>x</sup>, K. Andeen<sup>af</sup>, T. Anderson<sup>aw</sup>,  
I. Ansseau<sup>l</sup>, G. Anton<sup>x</sup>, M. Archinger<sup>ae</sup>, C. Argüelles<sup>n</sup>, J. Auffenberg<sup>a</sup>,  
S. Axani<sup>n</sup>, X. Bai<sup>an</sup>, S. W. Barwick<sup>aa</sup>, V. Baum<sup>ae</sup>, R. Bay<sup>g</sup>, J. J. Beatty<sup>r,s</sup>,  
J. Becker Tjus<sup>j</sup>, K.-H. Becker<sup>az</sup>, S. BenZvi<sup>ax</sup>, D. Berley<sup>q</sup>, E. Bernardini<sup>ba</sup>,  
A. Bernhard<sup>ah</sup>, D. Z. Besson<sup>ab</sup>, G. Binder<sup>h,g</sup>, D. Bindig<sup>az</sup>, E. Blaufuss<sup>q</sup>,  
S. Blot<sup>ba</sup>, C. Boehm<sup>ap</sup>, M. Börner<sup>u</sup>, F. Bos<sup>j</sup>, D. Bose<sup>ar</sup>, S. Böser<sup>ae</sup>,  
O. Botner<sup>ay</sup>, J. Braun<sup>ad</sup>, L. Brayeur<sup>m</sup>, H.-P. Bretz<sup>ba</sup>, S. Bron<sup>y</sup>,  
A. Burgman<sup>ay</sup>, T. Carver<sup>y</sup>, M. Casier<sup>m</sup>, E. Cheung<sup>q</sup>, D. Chirkin<sup>ad</sup>,  
A. Christov<sup>y</sup>, K. Clark<sup>at</sup>, L. Classen<sup>ai</sup>, S. Coenders<sup>ah</sup>, G. H. Collin<sup>n</sup>,  
J. M. Conrad<sup>n</sup>, D. F. Cowen<sup>aw,av</sup>, R. Cross<sup>ax</sup>, M. Day<sup>ad</sup>,  
J. P. A. M. de André<sup>v</sup>, C. De Clercq<sup>m</sup>, E. del Pino Rosendo<sup>ae</sup>,  
H. Dembinski<sup>aj</sup>, S. De Ridder<sup>z</sup>, P. Desiati<sup>ad</sup>, K. D. de Vries<sup>m</sup>,  
G. de Wasseige<sup>m</sup>, M. de With<sup>i</sup>, T. DeYoung<sup>v</sup>, J. C. Díaz-Vélez<sup>ad</sup>,  
V. di Lorenzo<sup>ae</sup>, H. Dujmovic<sup>ar</sup>, J. P. Dumm<sup>ap</sup>, M. Dunkman<sup>aw</sup>,  
B. Eberhardt<sup>ae</sup>, T. Ehrhardt<sup>ae</sup>, B. Eichmann<sup>j</sup>, P. Eller<sup>aw</sup>, S. Euler<sup>ay</sup>,  
P. A. Evenson<sup>aj</sup>, S. Fahey<sup>ad</sup>, A. R. Fazely<sup>f</sup>, J. Feintzeig<sup>ad</sup>, J. Felde<sup>q</sup>,  
K. Filimonov<sup>g</sup>, C. Finley<sup>ap</sup>, S. Flis<sup>ap</sup>, C.-C. Fösig<sup>ae</sup>, A. Franckowiak<sup>ba</sup>,  
E. Friedman<sup>q</sup>, T. Fuchs<sup>u</sup>, T. K. Gaisser<sup>aj</sup>, J. Gallagher<sup>ac</sup>, L. Gerhardt<sup>h,g</sup>,  
K. Ghorbani<sup>ad</sup>, W. Giang<sup>w</sup>, L. Gladstone<sup>ad</sup>, T. Glauch<sup>a</sup>, T. Glüsenskamp<sup>x</sup>,  
A. Goldschmidt<sup>h</sup>, J. G. Gonzalez<sup>aj</sup>, D. Grant<sup>w</sup>, Z. Griffith<sup>ad</sup>, C. Haack<sup>a</sup>,  
A. Hallgren<sup>ay</sup>, F. Halzen<sup>ad</sup>, E. Hansen<sup>t</sup>, T. Hansmann<sup>a</sup>, K. Hanson<sup>ad</sup>,  
D. Hebecker<sup>i</sup>, D. Heereman<sup>l</sup>, K. Helbing<sup>az</sup>, R. Hellauer<sup>q</sup>, S. Hickford<sup>az</sup>,  
J. Hignight<sup>v</sup>, G. C. Hill<sup>b</sup>, K. D. Hoffman<sup>q</sup>, R. Hoffmann<sup>az</sup>, K. Hoshina<sup>ad,as</sup>,  
F. Huang<sup>aw</sup>, M. Huber<sup>ah</sup>, K. Hultqvist<sup>ap</sup>, S. In<sup>ar</sup>, A. Ishihara<sup>o</sup>, E. Jacobi<sup>ba</sup>,  
G. S. Japaridze<sup>d</sup>, M. Jeong<sup>ar</sup>, K. Jero<sup>ad</sup>, B. J. P. Jones<sup>n</sup>, W. Kang<sup>ar</sup>,  
A. Kappes<sup>ai</sup>, T. Karg<sup>ba</sup>, A. Karle<sup>ad</sup>, U. Katz<sup>x</sup>, M. Kauer<sup>ad</sup>, A. Keivani<sup>aw</sup>,  
J. L. Kelley<sup>ad</sup>, A. Kheirandish<sup>ad</sup>, J. Kim<sup>ar</sup>, M. Kim<sup>ar</sup>, T. Kintscher<sup>ba</sup>,  
J. Kiryluk<sup>aq</sup>, T. Kittler<sup>x</sup>, S. R. Klein<sup>h,g</sup>, G. Kohnen<sup>ag</sup>, R. Koirala<sup>aj</sup>,  
H. Kolanoski<sup>i</sup>, R. Konietz<sup>a</sup>, L. Köpke<sup>ae</sup>, C. Kopper<sup>w</sup>, S. Kopper<sup>az</sup>,  
D. J. Koskinen<sup>t</sup>, M. Kowalski<sup>i,ba</sup>, K. Krings<sup>ah</sup>, M. Kroll<sup>j</sup>, G. Krückl<sup>ae</sup>,  
C. Krüger<sup>ad</sup>, J. Kunnen<sup>m</sup>, S. Kunwar<sup>ba</sup>, N. Kurahashi<sup>am</sup>, T. Kuwabara<sup>o</sup>,

---

\*Corresponding author:

Email address: markus.ackermann@desy.de (M. Ackermann)

M. Labare<sup>z</sup>, J. L. Lanfranchi<sup>aw</sup>, M. J. Larson<sup>t</sup>, F. Lauber<sup>az</sup>, D. Lennarz<sup>v</sup>,  
 M. Lesiak-Bzdak<sup>aq</sup>, M. Leuermann<sup>a</sup>, L. Lu<sup>o</sup>, J. Lünemann<sup>m</sup>, J. Madsen<sup>ao</sup>,  
 G. Maggi<sup>m</sup>, K. B. M. Mahn<sup>v</sup>, S. Mancina<sup>ad</sup>, M. Mandelartz<sup>j</sup>,  
 R. Maruyama<sup>ak</sup>, K. Mase<sup>o</sup>, R. Maunu<sup>q</sup>, F. McNally<sup>ad</sup>, K. Meagher<sup>l</sup>,  
 M. Medici<sup>t</sup>, M. Meier<sup>u</sup>, T. Menne<sup>u</sup>, G. Merino<sup>ad</sup>, T. Meures<sup>l</sup>, S. Miarecki<sup>h,g</sup>,  
 T. Montaruli<sup>v</sup>, M. Moulai<sup>n</sup>, R. Nahnhauser<sup>ba</sup>, U. Naumann<sup>az</sup>, G. Neer<sup>v</sup>,  
 H. Niederhausen<sup>aq</sup>, S. C. Nowicki<sup>w</sup>, D. R. Nygren<sup>h</sup>,  
 A. Obertacke Pollmann<sup>az</sup>, A. Olivas<sup>q</sup>, A. O'Murchadha<sup>l</sup>, T. Palczewski<sup>h,g</sup>,  
 H. Pandya<sup>aj</sup>, D. V. Pankova<sup>aw</sup>, P. Peiffer<sup>ae</sup>, Ö. Penek<sup>a</sup>, J. A. Pepper<sup>au</sup>,  
 C. Pérez de los Heros<sup>ay</sup>, D. Pieloth<sup>u</sup>, E. Pinat<sup>l</sup>, P. B. Price<sup>g</sup>,  
 G. T. Przybylski<sup>h</sup>, M. Quinnan<sup>aw</sup>, C. Raab<sup>l</sup>, L. Rädela<sup>a</sup>, M. Rameez<sup>t</sup>,  
 K. Rawlins<sup>c</sup>, R. Reimann<sup>a</sup>, B. Relethford<sup>am</sup>, M. Relich<sup>o</sup>, E. Resconi<sup>ah</sup>,  
 W. Rhode<sup>u</sup>, M. Richman<sup>am</sup>, B. Riedel<sup>w</sup>, S. Robertson<sup>b</sup>, M. Rongen<sup>a</sup>,  
 C. Rott<sup>ar</sup>, T. Ruhe<sup>u</sup>, D. Ryckbosch<sup>z</sup>, D. Rysewyk<sup>v</sup>, L. Sabbatini<sup>ad</sup>,  
 S. E. Sanchez Herrera<sup>w</sup>, A. Sandrock<sup>u</sup>, J. Sandroos<sup>ae</sup>, S. Sarkar<sup>t,al</sup>,  
 K. Satalecka<sup>ba</sup>, P. Schlunder<sup>u</sup>, T. Schmidt<sup>q</sup>, S. Schoenen<sup>a</sup>, S. Schöneberg<sup>j</sup>,  
 L. Schumacher<sup>a</sup>, D. Seckel<sup>aj</sup>, S. Seunarine<sup>ao</sup>, D. Soldin<sup>az</sup>, M. Song<sup>q</sup>,  
 G. M. Spiczak<sup>ao</sup>, C. Spiering<sup>ba</sup>, J. Stachurska<sup>ba</sup>, T. Stanev<sup>aj</sup>, A. Stasik<sup>ba</sup>,  
 J. Stettner<sup>a</sup>, A. Steuer<sup>ae</sup>, T. Stezelberger<sup>h</sup>, R. G. Stokstad<sup>h</sup>, A. Stöbl<sup>o</sup>,  
 R. Ström<sup>ay</sup>, N. L. Strotjohann<sup>ba</sup>, G. W. Sullivan<sup>q</sup>, M. Sutherland<sup>r</sup>,  
 H. Taavola<sup>ay</sup>, I. Taboada<sup>e</sup>, J. Tatar<sup>h,g</sup>, F. Tenholt<sup>j</sup>, S. Ter-Antonyan<sup>f</sup>,  
 A. Terliuk<sup>ba</sup>, G. Tešić<sup>aw</sup>, S. Tilav<sup>aj</sup>, P. A. Toale<sup>au</sup>, M. N. Tobin<sup>ad</sup>,  
 S. Toscano<sup>m</sup>, D. Tosi<sup>ad</sup>, M. Tselengidou<sup>x</sup>, C. F. Tung<sup>e</sup>, A. Turcati<sup>ah</sup>,  
 E. Unger<sup>ay</sup>, M. Usner<sup>ba</sup>, J. Vandenbroucke<sup>ad</sup>, N. van Eijndhoven<sup>m</sup>,  
 S. Vanheule<sup>z</sup>, M. van Rossem<sup>ad</sup>, J. van Santen<sup>ba</sup>, M. Vehring<sup>a</sup>, M. Voge<sup>k</sup>,  
 E. Vogel<sup>a</sup>, M. Vraeghe<sup>z</sup>, C. Walck<sup>ap</sup>, A. Wallace<sup>b</sup>, M. Wallraff<sup>a</sup>,  
 N. Wandkowsky<sup>ad</sup>, A. Waza<sup>a</sup>, Ch. Weaver<sup>w</sup>, M. J. Weiss<sup>aw</sup>, C. Wendt<sup>ad</sup>,  
 S. Westerhoff<sup>ad</sup>, B. J. Whelan<sup>b</sup>, S. Wickmann<sup>a</sup>, K. Wiebe<sup>ae</sup>,  
 C. H. Wiebusch<sup>a</sup>, L. Wille<sup>ad</sup>, D. R. Williams<sup>au</sup>, L. Wills<sup>am</sup>, M. Wolf<sup>ap</sup>,  
 T. R. Wood<sup>w</sup>, E. Woolsey<sup>w</sup>, K. Woschnagg<sup>g</sup>, D. L. Xu<sup>ad</sup>, X. W. Xu<sup>f</sup>,  
 Y. Xu<sup>aq</sup>, J. P. Yanez<sup>w</sup>, G. Yodh<sup>aa</sup>, S. Yoshida<sup>o</sup>, M. Zoll<sup>ap</sup>

<sup>a</sup>*III. Physikalisches Institut, RWTH Aachen University, D-52056 Aachen, Germany*

<sup>b</sup>*Department of Physics, University of Adelaide, Adelaide, 5005, Australia*

<sup>c</sup>*Dept. of Physics and Astronomy, University of Alaska Anchorage, 3211 Providence Dr., Anchorage, AK 99508, USA*

<sup>d</sup>*CTSPS, Clark-Atlanta University, Atlanta, GA 30314, USA*

<sup>e</sup>*School of Physics and Center for Relativistic Astrophysics, Georgia Institute of Technology, Atlanta, GA 30332, USA*

- <sup>f</sup>Dept. of Physics, Southern University, Baton Rouge, LA 70813, USA
- <sup>g</sup>Dept. of Physics, University of California, Berkeley, CA 94720, USA
- <sup>h</sup>Lawrence Berkeley National Laboratory, Berkeley, CA 94720, USA
- <sup>i</sup>Institut für Physik, Humboldt-Universität zu Berlin, D-12489 Berlin, Germany
- <sup>j</sup>Fakultät für Physik & Astronomie, Ruhr-Universität Bochum, D-44780 Bochum, Germany
- <sup>k</sup>Physikalisches Institut, Universität Bonn, Nussallee 12, D-53115 Bonn, Germany
- <sup>l</sup>Université Libre de Bruxelles, Science Faculty CP230, B-1050 Brussels, Belgium
- <sup>m</sup>Vrije Universiteit Brussel (VUB), Dienst ELEM, B-1050 Brussels, Belgium
- <sup>n</sup>Dept. of Physics, Massachusetts Institute of Technology, Cambridge, MA 02139, USA
- <sup>o</sup>Dept. of Physics and Institute for Global Prominent Research, Chiba University, Chiba 263-8522, Japan
- <sup>p</sup>Dept. of Physics and Astronomy, University of Canterbury, Private Bag 4800, Christchurch, New Zealand
- <sup>q</sup>Dept. of Physics, University of Maryland, College Park, MD 20742, USA
- <sup>r</sup>Dept. of Physics and Center for Cosmology and Astro-Particle Physics, Ohio State University, Columbus, OH 43210, USA
- <sup>s</sup>Dept. of Astronomy, Ohio State University, Columbus, OH 43210, USA
- <sup>t</sup>Niels Bohr Institute, University of Copenhagen, DK-2100 Copenhagen, Denmark
- <sup>u</sup>Dept. of Physics, TU Dortmund University, D-44221 Dortmund, Germany
- <sup>v</sup>Dept. of Physics and Astronomy, Michigan State University, East Lansing, MI 48824, USA
- <sup>w</sup>Dept. of Physics, University of Alberta, Edmonton, Alberta, Canada T6G 2E1
- <sup>x</sup>Erlangen Centre for Astroparticle Physics, Friedrich-Alexander-Universität Erlangen-Nürnberg, D-91058 Erlangen, Germany
- <sup>y</sup>Département de physique nucléaire et corpusculaire, Université de Genève, CH-1211 Genève, Switzerland
- <sup>z</sup>Dept. of Physics and Astronomy, University of Gent, B-9000 Gent, Belgium
- <sup>aa</sup>Dept. of Physics and Astronomy, University of California, Irvine, CA 92697, USA
- <sup>ab</sup>Dept. of Physics and Astronomy, University of Kansas, Lawrence, KS 66045, USA
- <sup>ac</sup>Dept. of Astronomy, University of Wisconsin, Madison, WI 53706, USA
- <sup>ad</sup>Dept. of Physics and Wisconsin IceCube Particle Astrophysics Center, University of Wisconsin, Madison, WI 53706, USA
- <sup>ae</sup>Institute of Physics, University of Mainz, Staudinger Weg 7, D-55099 Mainz, Germany
- <sup>af</sup>Department of Physics, Marquette University, Milwaukee, WI, 53201, USA
- <sup>ag</sup>Université de Mons, 7000 Mons, Belgium
- <sup>ah</sup>Physik-department, Technische Universität München, D-85748 Garching, Germany
- <sup>ai</sup>Institut für Kernphysik, Westfälische Wilhelms-Universität Münster, D-48149 Münster, Germany
- <sup>aj</sup>Bartol Research Institute and Dept. of Physics and Astronomy, University of Delaware, Newark, DE 19716, USA
- <sup>ak</sup>Dept. of Physics, Yale University, New Haven, CT 06520, USA
- <sup>al</sup>Dept. of Physics, University of Oxford, 1 Keble Road, Oxford OX1 3NP, UK
- <sup>am</sup>Dept. of Physics, Drexel University, 3141 Chestnut Street, Philadelphia, PA 19104, USA

<sup>an</sup>*Physics Department, South Dakota School of Mines and Technology, Rapid City, SD 57701, USA*

<sup>ao</sup>*Dept. of Physics, University of Wisconsin, River Falls, WI 54022, USA*

<sup>ap</sup>*Oskar Klein Centre and Dept. of Physics, Stockholm University, SE-10691 Stockholm, Sweden*

<sup>aq</sup>*Dept. of Physics and Astronomy, Stony Brook University, Stony Brook, NY 11794-3800, USA*

<sup>ar</sup>*Dept. of Physics, Sungkyunkwan University, Suwon 440-746, Korea*

<sup>as</sup>*Earthquake Research Institute, University of Tokyo, Bunkyo, Tokyo 113-0032, Japan*

<sup>at</sup>*Dept. of Physics, University of Toronto, Toronto, Ontario, Canada, M5S 1A7*

<sup>au</sup>*Dept. of Physics and Astronomy, University of Alabama, Tuscaloosa, AL 35487, USA*

<sup>av</sup>*Dept. of Astronomy and Astrophysics, Pennsylvania State University, University Park, PA 16802, USA*

<sup>aw</sup>*Dept. of Physics, Pennsylvania State University, University Park, PA 16802, USA*

<sup>ax</sup>*Dept. of Physics and Astronomy, University of Rochester, Rochester, NY 14627, USA*

<sup>ay</sup>*Dept. of Physics and Astronomy, Uppsala University, Box 516, S-75120 Uppsala, Sweden*

<sup>az</sup>*Dept. of Physics, University of Wuppertal, D-42119 Wuppertal, Germany*

<sup>ba</sup>*DESY, D-15735 Zeuthen, Germany*

---

## Abstract

The core mission of the IceCube Neutrino observatory is to study the origin and propagation of cosmic rays. IceCube, with its surface component IceTop, observes multiple signatures to accomplish this mission. Most important are the astrophysical neutrinos that are produced in interactions of cosmic rays, close to their sources and in interstellar space. IceCube is the first instrument that measures the properties of this astrophysical neutrino flux, and constrains its origin. In addition, the spectrum, composition and anisotropy of the local cosmic-ray flux are obtained from measurements of atmospheric muons and showers. Here we provide an overview of recent findings from the analysis of IceCube data, and their implications on our understanding of cosmic rays.

*Keywords:* IceCube, neutrinos, cosmic rays

---

## 1. Introduction

The first detection of high-energy neutrinos of cosmic origin in 2013 by the IceCube Neutrino Observatory [1] opened a new window to the non-thermal processes in our universe. Neutrinos interact only weakly with matter, and can escape energetic and dense astrophysical environments that are opaque to electromagnetic radiation. Moreover, at PeV energies, most of the universe is impenetrable to electromagnetic radiation, due to the scattering of high-energy photons ( $\gamma$  rays) on the cosmic microwave background and other radiation fields. Neutrinos therefore promise to provide unique insights into a large number of extreme astrophysical phenomena, ranging from stellar explosions to the accretion onto massive black holes. They are key messengers in the search for the origin of the highest energy cosmic rays (CRs). High-energy neutrinos may be produced through the interaction of CRs with ambient matter or radiation fields. Unlike the charged CRs they are neither deflected by magnetic fields, nor affected by matter or radiation fields on the way from the source to the Earth. They propagate undisturbed over cosmic distances, allowing us to observe an otherwise opaque high-energy universe and identify the sources in it.

Many candidate source classes exist that fulfill the basic requirements of accelerating CRs to the highest observed energies of about  $10^{20}$  eV. An upper limit on the reachable cosmic-ray (CR) energy in gradual acceleration processes, like e.g. Fermi acceleration, was noted by Hillas in [2]. Here, the size of the acceleration region has to be larger than the Larmor radius of the produced CRs, otherwise the particles are not confined for further acceleration. This notion led to the plot shown, in a modern adaptation, in Figure 1. The potential sources of ultra-high-energy CRs are many, including gamma-ray bursts (GRBs, e.g. [3]), young neutron stars and pulsars (e.g. [4]), the jets (e.g. [5]) and cores of active Galaxies (e.g. [6]), and galaxy merger shocks in clusters (e.g. [7]).

Cosmic neutrinos detected by IceCube can be used to probe the particle acceleration processes in these candidate source classes. Information can be deduced from the observed spectrum, the flavor composition and possible correlations of neutrino observations with known transients or sources. However, IceCube is more than “just” a cosmic neutrino detector. Using the surface array IceTop, and the thousands of muons from CR showers in the atmosphere that are registered every second in the in-ice array, IceCube can be used to study the spectrum, the composition and the isotropy of CRs that

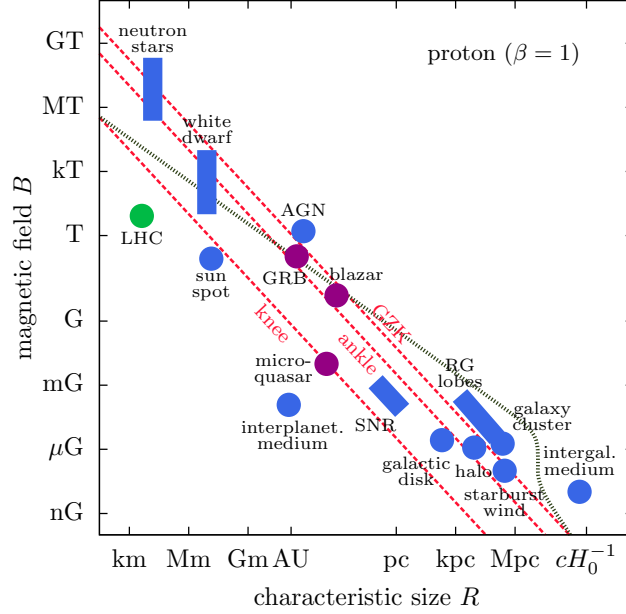


Figure 1: A modern adaption of the so called „Hillas plot” from [8]. It displays upper limits on the reachable CR energy dependent on the size of the acceleration region and magnetic field strength. The red lines indicate the upper limits due to the loss of confinement in the acceleration region for CRs at the *knee*, *ankle*, and the *Greisen-Zatsepin-Kuzmin (GZK)* cutoff [9, 10]. The dotted gray line corresponds to a second upper limit that arises from synchrotron losses in the sources and interactions in the cosmic photon background.

arrive at Earth at TeV and PeV energies. At PeV energies a transition in the CR spectrum and composition has been observed by many instruments (see review in [11]). This so called “knee”, is commonly attributed to Galactic sources being unable to accelerate CRs to energies above a few PeV per nucleon. Consequently, the composition of CRs changes at PeV energies, being dominated by increasingly heavier nuclei as the energy increases. The high statistics available in IceCube and the unique combination of a measurement of the electromagnetic and high-energy muon component of a CR air shower enable a precise measurement of both, spectral features and composition changes, in this energy range.

Even though CRs at TeV to PeV energies are efficiently deflected in the Galactic magnetic fields, the observation of small anisotropies in their arrival directions can give important clues to the existence and location of CR sources in our Galactic neighborhood. Such anisotropies have been observed by several instruments on the northern hemisphere [12, 13, 14, 15, 16, 17].

IceCube data now provide the most accurate measurement of this anisotropy in the Southern hemisphere at TeV and PeV energies, completing our picture of the arrival patterns of CRs on the sky.

After a short introduction to the IceCube neutrino telescope in section 2, we summarize the findings and insights that have been obtained in the first five years of IceCube operation on the properties (section 3) and the origin of the cosmic neutrino flux (sections 4 – 6). In each section we will also discuss the implications of these findings for the sources of high-energy CRs. We then describe the CR spectrum and composition measurements in section 7, and show and discuss recent results of the IceCube anisotropy measurement in section 8, before concluding this review in section 9.

## 2. The IceCube neutrino observatory

The IceCube Neutrino Observatory at the South Pole instruments approximately one cubic kilometer of the Antarctic ice sheet. It has been taking data in full configuration since spring 2011 with a duty cycle of more than 99%. IceCube is more than an order of magnitude larger than any experiments operating in the North (Baikal Deep Under-water Neutrino Telescope [18], Antares [19]). The planned KM3NeT and GVD detectors to be constructed in the Mediterranean sea and in the Lake Baikal in Siberia respectively, target a similar size as that of IceCube [20, 21].

IceCube consists of three components: the main IceCube array, the surface array IceTop, and a densely instrumented sub-array called DeepCore optimized for neutrinos with energies of a few tens of GeV. Optical sensors have been deployed at depths between 1450 m to 2450 m below the surface (see Figure 2). In total, 5160 digital optical modules (DOMs) are attached to 86 cables (strings) in a 3D hexagonal array optimally arranged to detect the Cherenkov photons emitted by charged particles traversing the ice.

All three components use the same instrumentation, design of DOMs and associated electronic readout [22, 23, 24]. The primary detector array is composed of 78 strings with a vertical separation of the DOMs of 17 m and an inter-string distance of about 125 m. With this geometry, IceCube detects neutrinos from the entire sky with energies above 100 GeV. Primary CRs interacting above the IceCube array, are detected with the CR air shower array IceTop that is operated in coincidence with the IceCube array [25]. IceTop is composed of 162 water tanks filled with clear ice and arranged in pairs at stations on the surface. Each station is 25 m from the top of

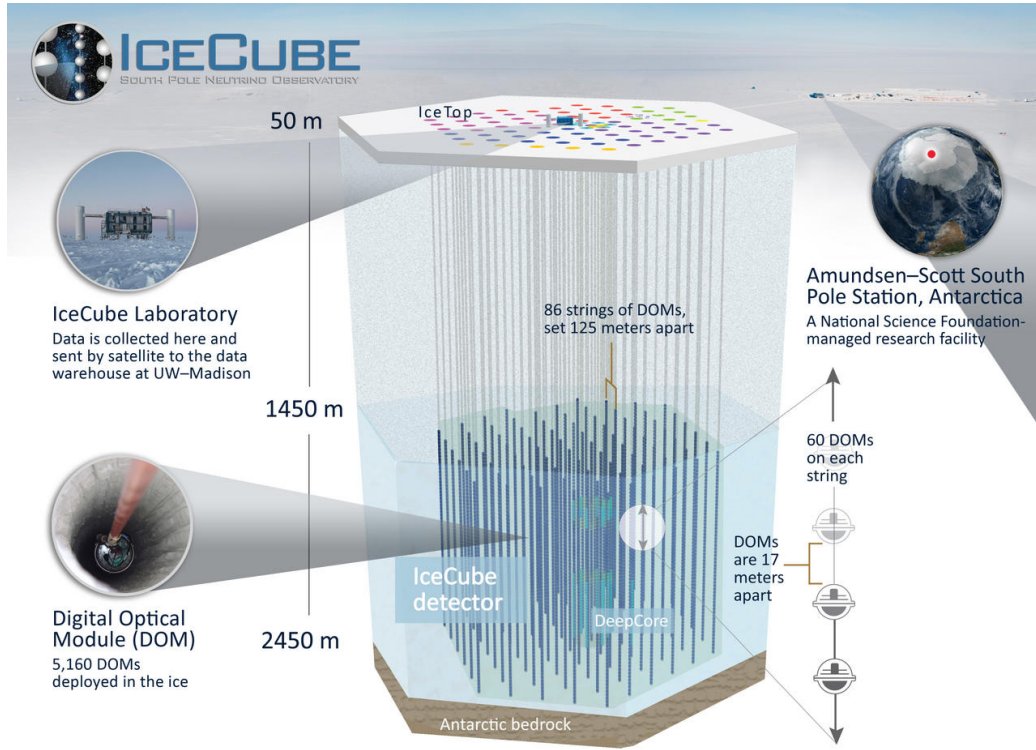


Figure 2: The IceCube Neutrino Observatory is composed of the IceCube array, the surface array IceTop, and the low-energy sub-array called DeepCore.

an IceCube string. Finally, DOMs have also been deployed in the central and deeper part of the IceCube array forming DeepCore, a more densely instrumented volume that extends IceCube operation to the lower energy regime of 10 GeV [26]. Here, the vertical DOM-to-DOM spacing is 7 m and the inter-string spacing is between 72 m and 42 m.

IceCube records events at a rate ranging between 2.5 kHz and 2.9 kHz [24]. The overwhelming majority of these events are muons from CR air showers that penetrate the ice and reach the depth of IceCube. Only about one in a million recorded events is from a neutrino interaction. Yet, this rate is sufficient for the collection of an unprecedentedly large sample of high-energy neutrinos ( $\sim 10^5 \text{ yr}^{-1}$ , predominantly of atmospheric origin) that offer a unique testbed for extreme astro- and particle physics.

Three main signatures can be distinguished for neutrino events in Ice-



Cube. “Track-like” events arise from muons produced in charged-current (CC) interactions of  $\nu_\mu$ . “Shower-like” events are generated in neutral-current (NC) interactions of all neutrino flavors, as well as in CC interactions of  $\nu_e$  (all energies) and  $\nu_\tau$  ( $E \leq 100$  TeV). High-energy  $\nu_\tau$  can produce a specific identifying signature, the so called “double-bang” events [27]. The hadronic shower at the  $\tau$  generation vertex and the shower produced at the  $\tau$  decay vertex can be separately identified when the tau track is longer than a few tens of meters ( $\gamma c\tau_\tau \approx 50$  m at 1 PeV).

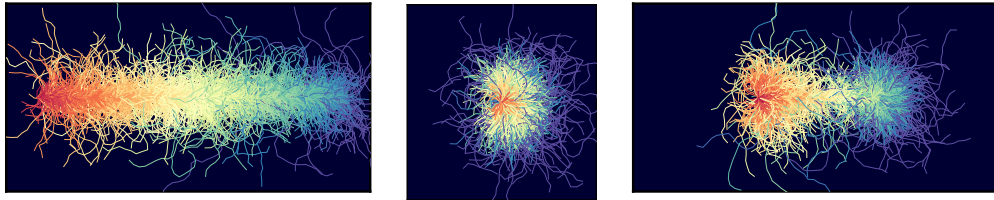


Figure 3: Simulation of Cherenkov light propagation in the ice for the three event signatures observable by IceCube: a track-like event (left), a shower-like event (middle) and a double-bang event (right). Each track marks the path of a photon. The colors indicate the relative time of the photons with respect to each other. Early photons are red, late photons are blue.

Figure 3 shows the propagation of Cherenkov photons in a simulation of the Antarctic ice for each described signature. Reconstruction of the physical properties of the neutrino that generated the event — direction, energy and flavor — is challenging due to the complex optical properties of the natural medium [28]. Scattering and absorption of photons in the ice mainly arises from deposits of minerals, soot and ash over more than a hundred thousand years. Therefore both, scattering and absorption lengths vary strongly with depth. Additionally, the flow of the antarctic ice shield introduces an anisotropy to the scattering. Melting and refreezing of the ice during DOM deployment locally changes the optical properties. In particular, for high energies above few tens of TeV, the reconstruction of event properties in IceCube is systematically limited due to these effects. Shower-like events can be reconstructed with an energy resolution of  $\sim 15\%$  [29], but the resolution of their arrival direction is rather poor at about  $15^\circ$ . On the other hand, the arrival direction of track-like events can be reconstructed with an accuracy better than  $1^\circ$ , but the energy of the neutrino can only indirectly be inferred from the energy deposited in the instrumented volume.

IceTop is located at an altitude of 2835 m above sea level, corresponding to an atmospheric overburden of  $690 \text{ g cm}^{-2}$ . Each tank is instrumented with two DOMs operating at different gains to provide a dynamic range from about 1/6 VEM (vertical equivalent muon<sup>1</sup>) to 1140 VEM. The IceTop surface array is triggered when six tanks in three stations register a signal in coincidence. The signal in the triggering tanks is typically dominated by the electromagnetic component of the air showers. For each trigger, both the surface detector and the in-ice signal are read out. IceTop has a small, central in-fill array with a threshold of about 100 TeV primary CR energy, while the regular-spaced array has a threshold of 300 TeV, recording air showers from primary CRs of energies up to about 2 EeV. Above this energy the rate becomes too low for analysis. The direction of events is reconstructed from the shower front arrival time, and has a resolution of  $\sim 0.3^\circ$  at 10 PeV. The energy is determined by fitting the lateral shower profile and using the signal size at a perpendicular distance from the shower core of 125 m. The resolution for protons at 30 PeV energy is 0.05 in  $\log_{10}(E/\text{GeV})$  [25].

### 3. Spectrum and flavor composition of astrophysical neutrinos

The majority of the neutrino events detected by IceCube are produced by CR interactions in the atmosphere. Figure 4 from Ref. [33] shows measurements of the flux of  $\nu_e$  as well as the more numerous  $\nu_\mu$ . The prompt component from decay of charmed mesons has not yet been detected. A hard astrophysical spectrum is expected to show up at high energy above the steeply falling atmospheric spectrum.

The first strong evidence for a cosmic neutrino component came from a search using data from May 2010 to April 2012 [35], where two shower-like events from interactions within the detector with energies above 1 PeV were discovered. A follow-up search for events starting in the detector with more than  $\simeq 30$  TeV deposited energy that utilized the same dataset identified 25 additional high-energy events [1]. The spectrum and zenith angle distribution of the events was incompatible with the hypothesis of an atmospheric origin at  $> 4\sigma$ . IceCube has since collected independent evidence for an astrophysical neutrino signal by analyzing different event signatures as described below, including shower-like and starting events at lower en-

---

<sup>1</sup>The energy deposited by a minimally ionizing muon vertically traversing the tank.

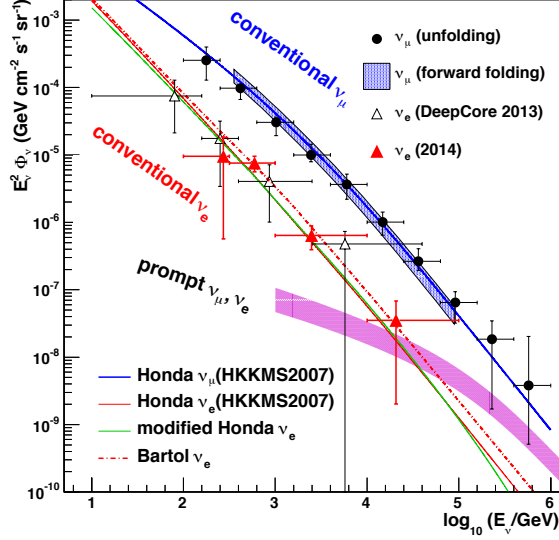


Figure 4: Spectrum of atmospheric neutrinos measured by IceCube:  $\nu_\mu$  forward folding from [30];  $\nu_\mu$  unfolding from [31];  $\nu_e$  from cascades in DeepCore [32];  $\nu_e$  with full IceCube [33]. The purple band shows the prompt flux expected from Ref. [34] after modification to account for the knee of the primary spectrum.

ergies as well as track-like events that interact outside the detector (called through-going events).

### 3.1. Starting Events

Neutrino interactions are identified in IceCube by searching for an interaction vertex within the instrumented volume. This search is sensitive to both shower-like and track-like events. Since the main background for this search is comprised of muons from CR air showers, the rejection strategy is to identify Cherenkov photons from a track entering the detector. For that, the outer parts of the instrumented volume are assigned to a “veto” region. An event is rejected if a certain number of Cherenkov photons are found in this veto region at earlier times than the photons produced at the interaction vertex. For a more detailed description see [36]. Data recorded between May 2010 and Apr 2014 have been analyzed to obtain a starting event sample with an energy threshold of  $E_\nu \sim 30$  TeV [37] including three shower-type events with energies in excess of 1 PeV. The first three years of this sample have also been used for an initial determination of the flavor ratio of astrophysical neutrinos [38]. If the size of the veto region is chosen to increase as

energy decreases, neutrino-induced shower-like and track-like events above a few TeV can be isolated from the background effectively. Using this approach, the starting event sample for two years (May 2010 to April 2012) has been extended to include lower-energy events down to  $E_\nu \sim 3$  TeV [39].

### 3.2. Shower-type events

An alternative strategy to distinguish neutrino-induced shower-type events from atmospheric backgrounds is to search for a spherical light pattern that fits the characteristics of Cherenkov light emission from a short<sup>2</sup> and well localized particle shower in or around the instrumented area. This allows identification of showers from neutrino interactions also in regions of the instrumented volume that serve vetoing purposes in the starting event searches and even to find showers nearby the instrumented volume. Data from May 2010 to Apr 2012 has been analyzed using this technique [40] selecting 172 shower-type events above  $E_\nu \sim 10$  TeV. Most of these events are not included in the previously described starting event sample of the same time period.

### 3.3. Through-going muons

Muons produced in CC neutrino interactions far outside the detector can still reach the instrumented volume to produce track-like events. Even at 1 TeV a muon can penetrate several kilometers of ice before it stops and decays. This allows observation of high-energy neutrino interactions from a much larger volume than the instrumented one, thereby substantially increasing the effective area of the detector. However, these so called “through-going” muons from neutrino interactions are indistinguishable from single high-energy muons produced in atmospheric showers. For this reason the Earth must be used as a filter to separate neutrino-induced from CR-induced muons. Muons that arrive from zenith angles above  $\sim 85^\circ$  must be produced in neutrino interactions, as muons produced in CR air showers could not penetrate far enough through the Earth and ice to reach the detector. Analyzing two years of IceCube data we found that the spectrum of neutrino-induced, upward muons shows a hardening above the steep atmospheric background consistent with an astrophysical flux [41]. The search for such muons has recently been extended to 6 years of IceCube data recorded

---

<sup>2</sup>For  $O(100)$  TeV hadronic and electromagnetic showers there is only a few meters distance between interaction vertex and shower maximum in ice, which is small compared to the typical distance between strings of 125 m.

between May 2009 and April 2015. The highest energy track found in this sample deposited 2.6 PeV of energy inside the volume of IceCube [42]. The search for through-going muons is sensitive to cosmic neutrinos above an energy of about  $E_\nu \sim 200$  TeV. At lower energies muons from the interactions of atmospheric  $\nu_\mu$  dominate over the cosmic component.

#### 3.4. Showers from $\nu_\tau$ interactions

A study to identify  $\nu_\tau$  interactions was performed on the IceCube data recorded between May 2010 and Apr 2013, searching for a double pulse signature within single optical modules that would be characteristic of a double shower from the interaction of the  $\nu_\tau$  and the decay of the  $\tau$  [43]. No such signature was found in 3 years of IceCube data, which is compatible with 0.54 expected events from simulations if cosmic neutrinos arrive at Earth with a flavor ratio of  $\nu_e : \nu_\mu : \nu_\tau = 1 : 1 : 1$ . While no  $\nu_\tau$  signature was detected the analysis helped to constrain the measurement of the flavor ratio in combination with the observation channels introduced above.

#### 3.5. Combined results

The combined analysis of IceCube data of all the detection channels described above<sup>3</sup> results in a spectrum between 27 TeV and 2 PeV consistent with an unbroken power law with a best-fit spectral index of  $-2.49 \pm 0.08$  [44, 45]. A slightly improved likelihood is obtained if the data is fit with a harder spectrum with a spectral index of  $-2.31$  and an exponential cutoff at 2.7 PeV. However, the improvement is not significant enough ( $\sim 1.2\sigma$ ) to claim the existence of such a cutoff, and both spectral models can describe the data reasonably well. The most recent analysis of high-energy muon tracks above 200 TeV shows a preferred spectral index of  $-2.13 \pm 0.13$  [42]. This result may be indicative of a spectral hardening (see Figure 5 left) at high energies.

The energy flux of cosmic neutrinos above 10 TeV is  $6.8 \times 10^{-10}$  ergs  $\text{cm}^{-2} \text{s}^{-1} \text{sr}^{-1}$ , based on the best fit power-law spectrum with exponential cutoff from the combined analysis. The spatial distribution of events on the sky is compatible with an isotropic distribution of sources, suggesting an

---

<sup>3</sup>Through-going muons are only included from the data taking periods between May 2009 and Apr 2012. An additional 3 years of through-going muons were analyzed only after the publication of the combined analysis. See also Figure 5.

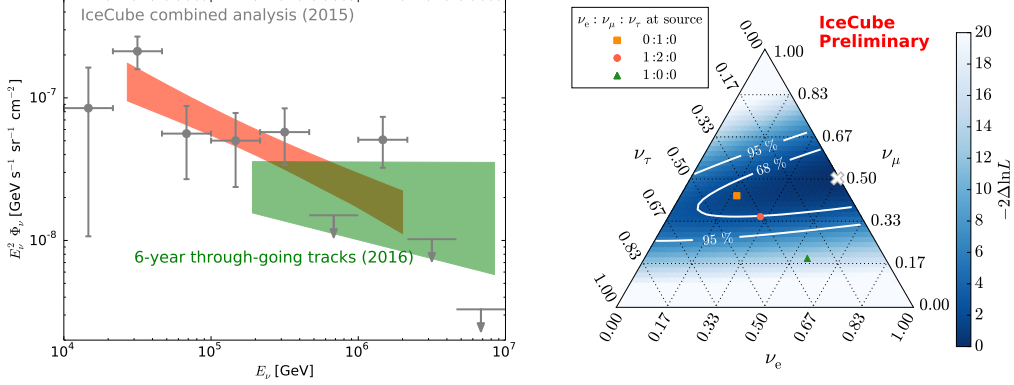


Figure 5: (Left) Spectrum of cosmic neutrinos measured in a combined analysis of all detection channels. The red bar indicates the best fit with a power-law spectral hypothesis. The gray points display the result for a fit of the neutrino flux in individual energy bands. A new measurement based on 6 years of through-going muons (green bar) that is sensitive at higher energies indicates a harder spectrum above few hundred TeV. (Right) Flavor constraints on the cosmic neutrino flux from the combined analysis [45] in comparison to different scenarios expected for neutrino production in astrophysical sources.

extragalactic origin of a substantial fraction of the observed cosmic neutrinos. Using the combined analysis, their flavor ratio can also be constrained. Figure 5 (right) shows the constraints on the relative contributions of the individual neutrino flavors to the cosmic neutrino flux. Typical astrophysical scenarios predict a flavor ratio at the production site of  $\nu_e : \nu_\mu : \nu_\tau = 1 : 2 : 0$  in case the neutrinos are produced by the decay of pions. Standard neutrino oscillations change this into an expected ratio of  $\nu_e : \nu_\mu : \nu_\tau \approx 1 : 1 : 1$  on arrival at Earth. If the secondary muons lose most of their energy before they can decay, e.g. due to strong magnetic fields in the sources, the production flavor ratio would be  $\nu_e : \nu_\mu : \nu_\tau = 0 : 1 : 0$  („muon-damped” scenario). The opposite scenario is also possible, i.e. the muons are accelerated substantially before they decay, shifting the flavor ratio towards  $\nu_e : \nu_\mu : \nu_\tau = 1 : 1 : 0$  [46]. In case the neutrinos are produced in the decay of neutrons a  $\nu_e : \nu_\mu : \nu_\tau = 1 : 0 : 0$  flavor ratio would be expected. The neutron decay origin is excluded at more than  $3\sigma$ , while the other production scenarios mentioned above are compatible with current observations.

## 4. Neutrino sources

### 4.1. Search for individual neutrino sources

In the case where the cosmic neutrino flux is dominated by bright individual sources, they should be detectable as a local excess of events on the sky with respect to the atmospheric neutrino and diffuse cosmic neutrino background. The sensitivity of a search for such features depends crucially on the precision by which the direction of the neutrinos can be reconstructed from the data, i.e. on the detector angular resolution.

Therefore, the best event signatures for this search are the through-going muons and track-like starting events with a median angular resolution of  $\leq 1^\circ$ . The starting events are particularly important for the analysis of the Southern hemisphere sources where the strong background of muon bundles from CR air showers requires a very high energy threshold for the acceptance of through-going tracks.

The most recent analysis [47] combines seven years of IceCube data recorded between May 2008 to Apr 2015, corresponding to a livetime of 2431 days of through-going muons, and 1715 days of track-like starting events<sup>4</sup>. In total 422791 through-going muons from the Northern hemisphere, 289078 through-going muons from the Southern hemisphere and 961 starting tracks have been identified. The overwhelming majority of the muons from the North originate from atmospheric neutrinos, while most of the muons from the South arise from muons and muon bundles created in CR air showers. The acceptance of background events vs. signal neutrinos has been optimized to achieve the optimal sensitivity for a detection for a range of potential point source spectra. The datasets are analyzed using a maximum likelihood technique to find one or more localized excesses over the diffuse backgrounds that correspond to the neutrino sources.

Figure 6 presents the discovery potential for point sources at various declinations ( $\delta$ ) achieved in this analysis. The most sensitive energy range changes with declination and is  $> 1$  PeV for  $\delta = -60^\circ$ , between 100 TeV and 1 PeV at the horizon, and below 100 TeV at  $\delta = 60^\circ$ . The generally lower discovery potential for sources at  $\delta = -60^\circ$  is due to the limited overburden of ice above the detector which limits the amount of target material,

---

<sup>4</sup>Starting events were not available before May 2010 while IceCube was under construction. The through-going muon sample contains data from the partially completed IceCube detector in its 40 and 59 string configurations.

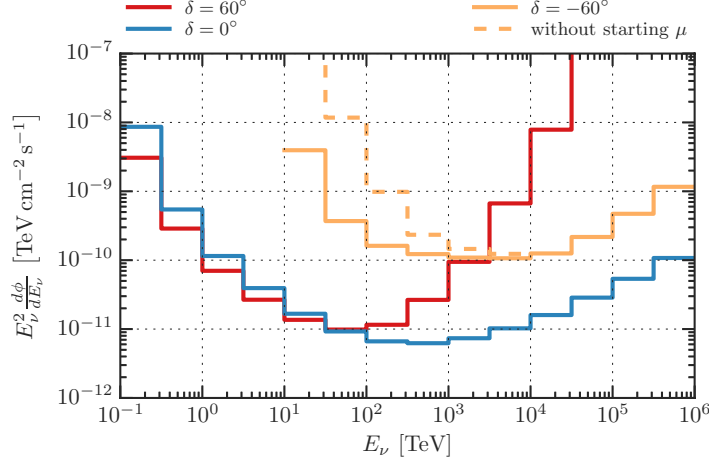


Figure 6: Differential discovery potential of the point source search [47] for various zenith angles. Shown is the neutrino flux from a point source over half a decade in energy that would lead to a  $5\sigma$  discovery in the current search for 50% of statistical realizations. The dashed line indicates the sensitivity if starting events would be ignored. A power-law spectrum with an index of 2 is assumed for the neutrino flux within a single energy bin.

and the high-energy threshold for accepting muons thus reducing the strong background from CR air showers. For sources at a declination of  $\delta = 60^\circ$ , neutrinos with energies  $>100$  TeV are increasingly absorbed in the Earth, reducing the discovery potential at high energies.

#### 4.2. Flux upper limits derived from IceCube data

No indication for a neutrino point source has been found in the IceCube data so far and Figure 7 summarizes the results of the search described above. The map shows the p-values for each point in the sky giving the local probability that an excess is a fluctuation of the background. To estimate the significance of the lowest observed p-values on each hemisphere, event samples have been generated with the right ascension coordinates randomized. These samples have been analyzed in the same way as the original dataset. The distribution of the minimum p-values in the samples can then be compared to that observed in the data. The fraction of randomized samples with a lower p-value than the lowest observed p-value in the data is 29% for the Northern sky, and 17% for the Southern sky. That is, the observations are compatible with fluctuations of the diffuse background.



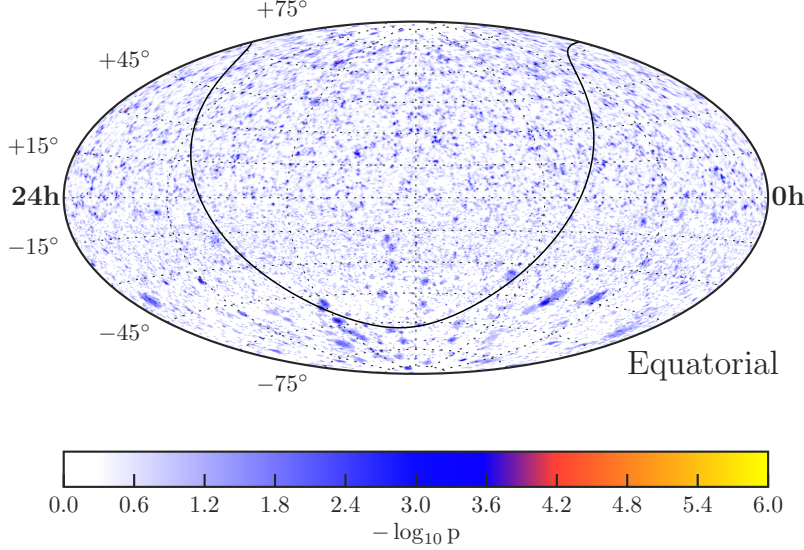


Figure 7: Map of p-values representing the local probability that an excess of events at a given position in the sky is due to a fluctuation of the expected background [47].

Additionally, the known locations of promising individual neutrino source candidates have been tested. These candidates have been selected based on model calculations and/or the observation of non-thermal emission features in the electromagnetic spectrum. None of the tested candidates shows a significant excess of neutrino events around its position. In Figure 8 the neutrino flux upper limits summarize the result from this non-observation. Also shown is the discovery potential, i.e. the flux that would lead to a  $5\sigma$  discovery of a source in 50% of the statistical representations (without any corrections for multiple trials).

A comparison of the flux upper limits to a selection of individual source emission models is shown in Figure 9. The flux limits have to be calculated specifically for the predicted neutrino spectra based on the declination and energy dependent instrument response. The two panels show examples of recent models of the neutrino emission from blazars [49, 50]. The predicted spectra are compared to the flux upper limits derived from IceCube data. For some of the sources the limits are on the level of the calculated flux and start to constrain the parameter space of such models. More details about the search presented above can be found in [47]. In addition, dedicated tests were performed to find transient sources [51] and sources that are spatially

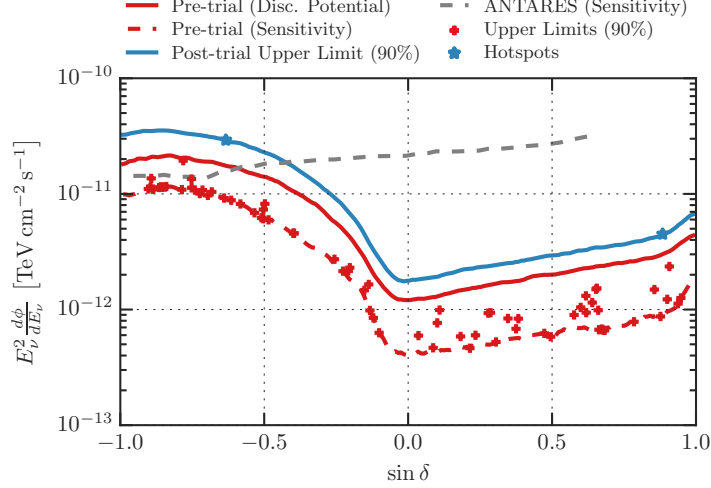


Figure 8: Neutrino flux upper limits for various source candidates, sensitivities and discovery potential as a function of the source declination [47]. The red dots indicate the 90% CL flux upper limits for individual candidate sources. The dashed red line represents the corresponding sensitivity at the respective declination. The gray dashed line indicates the sensitivity of the Antares neutrino telescope [48]. The blue line shows the flux upper limit that corresponds to the lowest observed p-value in each half of the sky as a function of declination (the actual declination of the observed spots is indicated by a star). A power-law spectrum with an index of 2 is assumed when generating the limits.

extended [52]<sup>5</sup>, both yielding null results.

#### 4.3. Constraints on astrophysical source populations

The observation of an isotropic flux of astrophysical neutrinos seems to be at odds with the non-observation of individual neutrino point sources in the same data [47, 48, 51, 53, 54, 55, 56, 57]. However, the two results are consistent if the diffuse flux is dominated by many weak sources that are individually below the point source sensitivity [58, 59, 60]. This argument can be turned into a lower limit on the abundance of extragalactic neutrino sources, that we outline in the following.

The (quasi-)diffuse flux of neutrinos ( $\phi$  in units of  $\text{GeV}^{-1} \text{s}^{-1} \text{cm}^{-2} \text{sr}^{-1}$ ) originating in multiple cosmic sources is simply given by the redshift inte-

<sup>5</sup>These searches so far did not use the full May 2008 – Apr 2015 dataset described above.

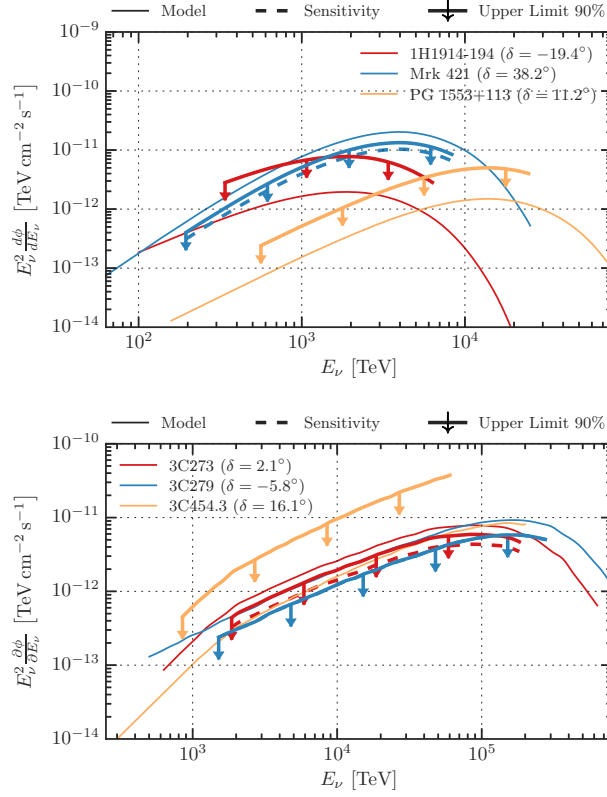


Figure 9: Experimental upper limits on the neutrino flux [47] in comparison to predictions for blazars in [49, 50].

gral [61]

$$\phi_\nu(E_\nu) = \frac{c}{4\pi} \int_0^\infty \frac{dz}{H(z)} \mathcal{Q}_\nu(z, (1+z)E_\nu). \quad (1)$$

Here,  $H(z)$  is the redshift dependent Hubble expansion rate and  $\mathcal{Q}_\nu$  is the spectral emission rate density of neutrinos. To a first approximation, we decompose the emission rate density into  $\mathcal{Q}(z, E) = \rho(z)Q_\nu(E)$  where  $\rho$  is the source density and  $Q_\nu$  is the emission rate per source. Note, this approximation assumes neutrino sources are standard candles and does not allow for luminosity distributions. However, these aspects can be included in a more detailed treatment.

The Hubble expansion in the redshift integral of Eq. (1) limits the contribution of sources beyond the Hubble horizon  $c/H_0$ . The redshift dependence

of the source distribution can then be parametrized by the energy dependent quantity

$$\xi_z(E) = \int_0^\infty dz \frac{H_0}{H(z)} \frac{\mathcal{Q}_\nu(z, (1+z)E)}{\mathcal{Q}_\nu(0, E)}, \quad (2)$$

which is typically of  $\mathcal{O}(1)$ . For the special case of power-law spectra  $\mathcal{Q}_\nu(E) \propto E^{-\gamma}$ , this quantity becomes energy independent and, for simplicity, we will assume the case  $\gamma = 2$  in the following. For instance,  $\xi_z \simeq 2.4$  if we assume that the source evolution follows the star-formation rate (SFR) [62, 63] or  $\xi_z \simeq 0.5$  for a source distribution with no evolution in the local ( $z < 2$ ) Universe.

Based on the observed per-flavor diffuse flux at the level of  $E^2\phi_\nu \simeq 10^{-8} \text{ GeV}^{-1} \text{ s}^{-1} \text{ cm}^{-2} \text{ sr}^{-1}$  we can then estimate the average neutrino point source luminosity via Eq. (1) as  $E^2\mathcal{Q}_\nu(0, E) \simeq (4\pi H_0/c\xi_z\rho_0)E^2\phi_\nu$ . On the other hand, for a homogeneous source distribution  $\rho_0$  in the local Universe we expect that the brightest source contributes with a flux  $E^2\phi_\nu^{\text{PS}} \simeq 0.55(f_{\text{sky}}\rho_0)^{2/3}E^2\mathcal{Q}_\nu$ , where  $f_{\text{sky}} \leq 1$  is the effective sky coverage of the observatory (see Ref. [61] for details). This translates into a point source flux given by:

$$E^2\phi_\nu^{\text{PS}} \simeq 1.9 \times 10^{-12} \left(\frac{\xi_z}{2.4}\right)^{-1} \left(\frac{f_{\text{sky}}}{0.5}\right)^{\frac{2}{3}} \left(\frac{\rho_0}{10^{-8} \text{ Mpc}^{-3}}\right)^{-\frac{1}{3}} \frac{\text{TeV}}{\text{cm}^2 \text{ s}}. \quad (3)$$

Presently, the sensitivity of IceCube to continuous point source emission in the Northern Hemisphere is at the level of  $E^2\phi_{\nu_\mu+\bar{\nu}_\mu}^{\text{PS}} \sim 10^{-12} \text{ TeV cm}^{-2} \text{ s}^{-1}$  (see section 4.2 and figure 8). This is already putting some tension on very rare source candidates like blazars ( $\rho_0 \lesssim 10^{-7} \text{ Mpc}^{-3}$ ). In fact, a dedicated IceCube analysis looking for the combined neutrino emission from Fermi LAT identified blazars [64] places an upper limit on their contribution that is at the level of about 25% of the observed flux. Figure 10 shows the maximum contribution from blazars in the 2LAC catalog to the observed cosmic neutrino flux for two different spectral hypotheses. If additionally a strict proportionality is assumed between the emitted power at GeV energies and in TeV neutrinos, the 2FGL blazars can contribute less than 10% to the observed flux (e.g. for sources for which the high-energy emission is dominated by pion-decay processes).

A similar line of argument can also be applied to transient sources [61]. Here, the experimental livetime does not increase the individual emission of

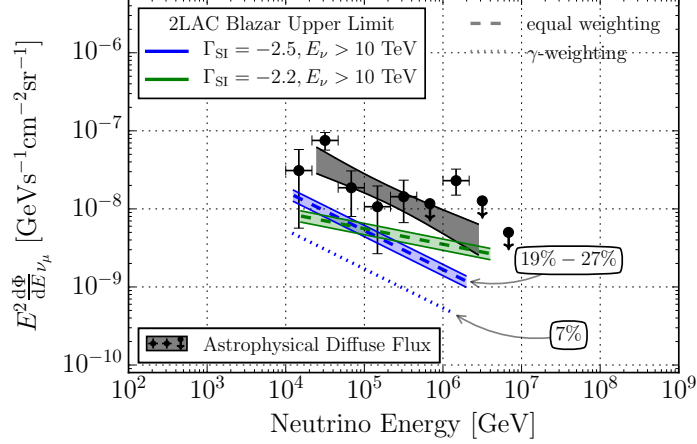


Figure 10: Upper limit on the contribution of Fermi LAT observed blazars (2LAC catalog) to the cosmic neutrino flux, shown for two different power-law spectra for the neutrino flux with indices of 2.5 and 2.2, respectively [64]. The width of the upper limit band indicates the dependence on the relative distribution of neutrino luminosities in the blazar sample if no strict proportionality is assumed between the  $\gamma$ -ray and neutrino luminosity of the source. The dotted line indicates the upper limit in case such proportionality is considered.

transients, but the total size of the source sample with local burst density  $\dot{\rho}_0$ . For instance, the contribution of gamma-ray bursts ( $\dot{\rho}_0 \simeq 10^{-9} \text{ Mpc}^{-3} \text{ yr}^{-1}$ ) to the diffuse emission is limited to less than 10% due to IceCube’s strong limit on the prompt neutrino emission of GRBs coincident with the gamma-ray signal [56].

#### 4.4. Neutrinos from the propagation of ultra-high energy CRs

The CR spectrum extends to energies far above  $10^{18} \text{ eV}$ . These ultra-high energy (UHE) CRs are believed to be accelerated in extragalactic sources since Galactic magnetic fields are too weak to sufficiently confine the UHE CRs. Candidate sources include GRBs, active galactic nuclei or galaxy clusters (see Figure 1).

The propagation of UHE CRs over cosmic distances makes them susceptible to interactions with cosmic backgrounds. In particular, photo-pion production of CR nuclei on the cosmic microwave background (CMB) with a local density of about  $410 \text{ cm}^{-3}$  becomes resonant at CR nucleon energies of about  $7 \times 10^{11} \text{ GeV}$ . This leads to a strong suppression of CR protons

beyond an energy at about  $E_{\text{GZK}} \simeq 5 \times 10^{19}$  eV, which is known as the GZK suppression [9, 10].

The neutrinos from the decaying pions are the so called *cosmogenic* or *GZK* neutrinos [65]. For proton-dominated UHE CR models, the expected flux peaks at EeV energies and is expected to be equally distributed between neutrino flavors after propagation [66, 67, 68]. This flux is considered a *guaranteed* contribution to high-energy neutrino fluxes since it does not rely on specific neutrino production mechanisms in CR sources. However, even in the simplest case of proton-dominated models, the flux depends on the unknown UHE CR source redshift evolution function and maximal energy cutoff of the proton spectra.

The largest contributions are predicted in proton models with a low energy cross-over between Galactic and extragalactic CRs, which typically require a strong redshift evolution of sources to fit the data [69, 70, 71, 72]. However in this case the related production of high energy  $\gamma$  rays, electrons and positrons predict a strong extragalactic diffuse  $\gamma$ -ray background [73, 74, 75, 76, 77, 78] in excess of the observations with the Fermi LAT [79, 80].

Proton-dominated UHE CR models generally are in reach of present neutrino observatories. However, the large experimental uncertainties on the relative contribution of heavier nuclei translates into large uncertainties in the cosmogenic neutrino predictions. The simple reason is that if the UHE CR spectrum is dominated by heavy nuclei with atomic mass number  $A$ , then the resonant interaction of CR nucleons with the CMB is shifted to higher CR energies,  $(A/56) \times 4 \times 10^{13}$  GeV. For the extreme case of iron this would shift the required CR energies to a level beyond the observed CR spectrum.

In the context of an increased threshold for GZK neutrino production by heavy nuclei, additional cosmic radiation backgrounds with higher photon energies can become a more important target. The extragalactic background light (EBL) in the infrared, optical and ultra-violet are included in most GZK neutrino predictions including heavy nuclei [76, 81, 82, 83, 84, 85, 86, 87, 88]. In general, these EBL neutrino predictions shift the peak neutrino production to the 1-10 PeV range but at an absolute level that is below present experimental sensitivities. As in the case of the proton dominated model, the cosmogenic neutrino prediction depends also on maximal energies and evolution of models. An estimate of a lower limit of these pessimistic models was given in Ref. [89].

The search for cosmogenic neutrinos is one of the standard analyses of IceCube. At EeV energies, where the emission is expected to peak, there are

practically no background events from atmospheric CR interactions. However, even after seven years of observation, no signal consistent with the expected emission spectra of various GZK models has been detected [90]. These limits now start to exclude some of the more optimistic scenarios of UHE CRs, dominated by light nuclei and/or strong source evolution (see also Ref. [77]). In addition to constraining propagation, the non-observation of neutrinos with energies above a few PeV sets upper limits on the cumulative emission of neutrinos from astrophysical sources in the energy range between 10 PeV and 1 EeV. These limits are comparable to predictions from blazar [91, 92] and Pulsar models [4].

## 5. Neutrino transients

### 5.1. *Gamma-Ray Bursts*

GRBs are intense  $\gamma$ -ray flashes lasting from fractions of a second to tens of minutes. During their prompt emission phase they are the brightest explosions in the Universe reaching isotropic-equivalent energies of up to  $10^{54}$  ergs. They are likely powered by the core-collapse of a very massive star or the merger of two compact objects. Their locations are distributed isotropically and they have been measured up to a redshift  $z = 8$ . GRBs have been proposed as the sources of the highest-energy CRs [93]. The central engine produces highly relativistic collimated jets, which are predicted to host internal shocks, where particles are efficiently accelerated to high energies. In hadronic scenarios, accelerated protons interact with ambient synchrotron photons and produce high-energy neutrinos. The neutrino emission is expected to be collimated and in temporal coincidence with the prompt  $\gamma$ -ray emission.

A search for high-energy neutrinos detected by IceCube from the locations of 807 GRBs in coincidence with their prompt  $\gamma$ -ray emission did not find a significant excess compared to background expectations [94]. This result provides tight constraints on models of neutrino and ultra-high-energy CR production in GRBs. Current models assuming acceleration of protons [3] and models assuming CR production through the decay of escaping neutrons [95] are excluded at 90% confidence (see Figure 11). However, models assuming multiple emission regions predict a neutrino flux below our current sensitivity [96].

Limits on the neutrino flux normalization allow us to constrain the contribution of  $\gamma$ -ray bright GRBs to less than 1% of the observed cosmic neutrino

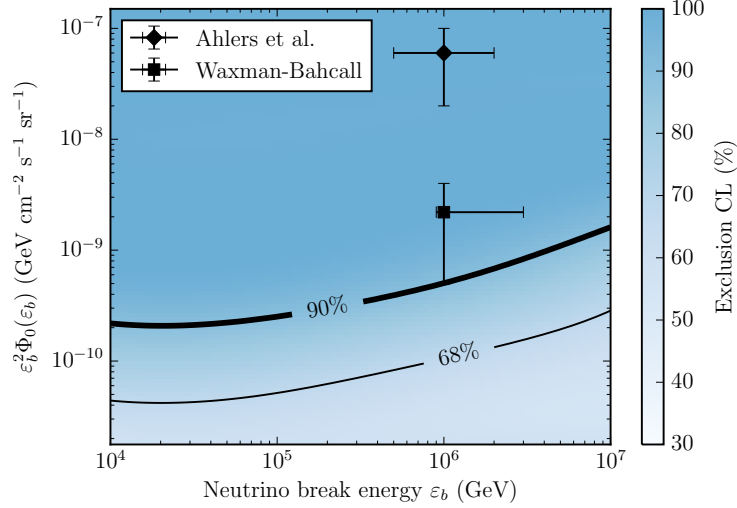


Figure 11: Limits on GRB model parameters adopted from Aartsen et al. [94].

flux [94]. However, a possibly large population of choked-jet GRBs with low  $\gamma$ -ray luminosity might contribute a larger fraction of the astrophysical neutrino flux. Choked jets may explain trans-relativistic supernovae (SNe) and low-luminosity GRBs, giving a unified picture of GRBs and GRB-SNe [97]. This scenario can be tested by correlating high-energy neutrinos with SNe.

### 5.2. Supernovae

Analogous to GRBs, high-energy neutrino production is predicted from SNe hosting mildly relativistic jets, which get choked in the envelope of the star [98, 99, 100]. Preferred candidates for choked-jet SNe are Type Ic SNe [101]. The neutrino emission is expected at the time of the SN explosion and to last  $\mathcal{O}(10\text{s})$ , comparable to the typical GRB duration. Other models predict neutrino emission from SNe exploding in a dense circum-stellar medium (CSM) [102, 103]. Neutrinos are produced in the interactions of the SNe ejecta with the dense medium on time scales of months to years.

Supernovae are most easily discovered at optical wavelengths. However, current optical surveys cover only limited regions of the sky or do not go very deep. To overcome this limitation, the IceCube collaboration set up an optical follow-up program for neutrino events of interest [104] in 2008. The IceCube data are processed in real-time and the most interesting neutrino events are selected to trigger observations with optical telescopes aiming for the detection of an optical counterpart.



The Palomar Transient Factory (PTF) [105] found a Type IIn SN, triggered by two track-like IceCube events which arrived within 1.6 s [106], at a location compatible with the direction of the neutrinos. Type IIn SNe are likely powered by interactions of the ejecta with a dense circumstellar medium, and are candidate neutrino sources with an expected duration of the neutrino emission of several months. Unfortunately, it turned out that the SN was already 160 days old at the time of the neutrino detection. It is very unlikely that two neutrinos arrive within 1.6 s, so late after the SN explosion. The observation can therefore be considered a chance coincidence. It nevertheless shows the potential of follow-up observations to reveal neutrino source candidates that would otherwise remain undetected. A dedicated search for neutrinos from an ensemble of Type IIn SNe observed independently of IceCube alerts is currently under development to test the possibility of long-term neutrino emission from Type IIn SNe.

Another supernova was found in a follow-up of a public IceCube alert (see Sec. 5.4). The Pan-STARRS optical telescope found a SN – possibly of type Ic – with an explosion time consistent with the arrival time of a high-energy neutrino [107]. An analysis is currently in progress to investigate in detail the SN type classification, as well as the probability for a chance coincidence between such a SN and a high-energy neutrino.

### 5.3. Blazar flares

In addition to the optical follow-up program, IceCube has operated a  $\gamma$ -ray follow-up program [108] since March 2012, which alerts the Cherenkov telescopes MAGIC<sup>6</sup> and VERITAS<sup>7</sup>. This program is aiming for the detection of neutrinos in coincidence with  $\gamma$ -ray flares from blazars. A predefined list of known variable  $\gamma$ -ray sources is monitored by IceCube for an excess in neutrinos on time scales of up to three weeks. So far, no  $\gamma$ -ray flare was detected in coincidence with a neutrino excess. A hint for neutrino production in blazar flares was claimed in [109], where a PeV neutrino shower event was found in spatial and temporal coincidence with a  $\gamma$ -ray outburst from the blazar PKS B1424-418.

---

<sup>6</sup><http://magic.mppmu.mpg.de>

<sup>7</sup><http://veritas.sao.arizona.edu>

#### 5.4. *Public IceCube alerts*

Since the spring of 2016 a real-time selection for high-energy single track events with high probability of being of astrophysical origin is in place. An expected rate of four high-energy starting track events (HESE) and four extreme high-energy through-going track events (EHE) are selected per year and published in real-time through the Astrophysical Multi-messenger Observatory Network (AMON) [110] via the Gamma-Ray Coordinate Network (GCN<sup>8</sup>). The first public neutrino alerts were followed up by various instruments in several wavelengths ranging from optical to  $\gamma$ -ray bands. A detailed overview of the different IceCube real-time channels can be found in [111].

#### 5.5. *Gravitational Wave Follow-Up*

The detection of the first gravitational wave (GW) event by the advanced LIGO detectors<sup>9</sup> in September 2015 [112] was accompanied by a broad multi-messenger follow-up program looking for the detection of a counterpart to the GW signal. IceCube and Antares searched their data in a  $\pm 500$  s time window centered on the GW event for high-energy neutrinos [113]. No neutrino event was detected by Antares while IceCube found three events in the time window, which is consistent with background expectations. Those events were not in spatial coincidence with the GW position as shown in Figure 12. Given the absence of a coincident signal, an upper limit on the total energy radiated in neutrinos of  $5.4 \times 10^{51}$  -  $1.3 \times 10^{54}$  erg was derived assuming an energy spectrum following  $dN/dE \sim E^{-2}$ . Both of the distinct sky regions (see Figure 12) are considered in the limit calculation to provide an inclusive range.

### 6. Neutrinos from cosmic-ray interactions in the Galactic plane

Cosmic rays up to a few PeV are believed to originate in Galactic sources. At this energy the CR spectrum shows a break, the so-called CR *knee*, which could indicate that the sources have reached their maximal acceleration energy for the lightest nuclei. It has long been speculated that Galactic core-collapse SNe, which occur at a rate of about 3 per century, could be responsible for the observed CR density [114]. These cataclysmic events produce

---

<sup>8</sup><http://gcn.gsfc.nasa.gov>

<sup>9</sup><http://ligo.org>

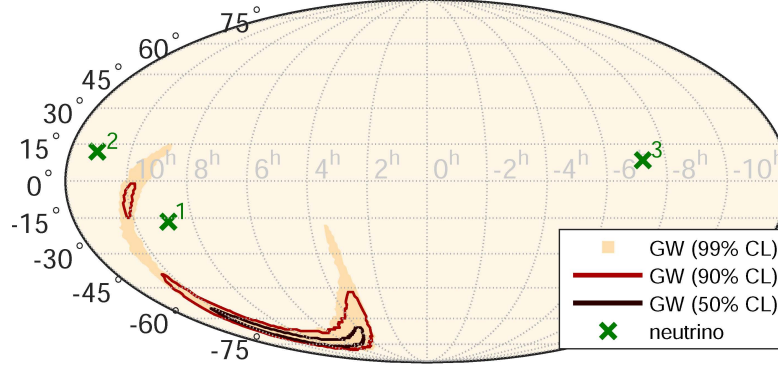


Figure 12: Skymap of the probability density contours of the GW event in equatorial coordinates together with the high-energy neutrino candidates detected by IceCube within a  $\pm 500$  s time window centered on the GW event. Figure adopted from Adrian-Martinez et al. [113].

ejecta with kinetic energy of the order of  $10^{51}$  erg per SN explosion. Diffuse shocks that form as the ejecta run into the ambient medium could accelerate particles and transfer a significant fraction of this kinetic energy to a non-thermal population of cosmic rays.

Interactions of CRs with gas during their acceleration in the source or during their passage through nearby molecular clouds can lead to the production of charged and neutral pions. In the decay of neutral pions,  $\pi^0 \rightarrow \gamma\gamma$ , these sources could be visible via their  $\gamma$ -ray emission. Indeed, recent observation of Fermi-LAT [115] indicate, that the  $\gamma$ -ray spectra of two Galactic supernova remnants, W44 and IC 443, show evidence for a characteristic rise in the spectra below  $\sim 200$  MeV resulting from pion decay. The corresponding decay of charged pions, e.g.  $\pi^+ \rightarrow \mu^+ \nu_\mu$  followed by  $\mu^+ \rightarrow e^+ \nu_e \bar{\nu}_\mu$ , would be visible as high-energy neutrino emission. It has also been suggested that the injected  $e^\pm$  from the production and decay of charged pions in the acceleration region would result in hard emission of  $e^\pm$  [116, 117] that could be responsible for the steep rise of the positron fraction in Galactic CRs above 10 GeV observed with PAMELA [118], Fermi-LAT [119], and AMS [120]. The associated neutrino emission could be observable in IceCube [121].

After emission from their sources, CRs start to diffuse through the Galactic magnetic fields. This process has two effects. First, the arrival directions of the CRs become highly isotropized and obscure the position of the sources. Second, the diffusion process softens the spectra compared to the initial emis-

sion spectrum due to the enhanced loss of particles at higher energies. Diffusion also implies a rather smooth distribution of CRs throughout the Milky Way and therefore the local CR density,  $n_{\text{CR}} \simeq 4\pi\phi_{\text{CR}}/c$ , can be used as a proxy of the average density. The interaction of these CRs with gas in the vicinity of the Galactic plane then guarantees a diffuse Galactic emission of neutrinos and  $\gamma$  rays [122, 123, 124, 125, 126, 127, 128, 129].

The local emission rate of neutrinos (per flavor) from Galactic CR interactions can be estimated by the local nucleon density  $n_N$  as

$$E_\nu^2 Q_\nu(E_\nu) \simeq \frac{1}{6} cn\kappa\sigma_{pp} [E_N^2 n_N(E_N)]_{E_N=20E_\nu} , \quad (4)$$

where  $\sigma_{pp}$  is the inelastic proton-proton cross section with inelasticity  $\kappa \simeq 0.5$  [130, 131]. The  $1/6$  factor accounts for the per flavor emission ( $\simeq 1/3$ ), for the total neutrino energy fraction in the charged pion decay ( $\simeq 3/4$ ) and for the charged pion fraction in  $pp$  collisions ( $\simeq 2/3$ ). The neutrino energy is related to the energy of CR nucleons ( $N$ ) as  $E_\nu \simeq E_N/20$ . The target gas density  $n$  is mostly concentrated along the Galactic plane, but can also show high-latitude fluctuations from atomic and molecular gas clouds. The left plot of Figure 13 shows the predicted intensity of the diffuse emission from [129] in terms of Galactic coordinates. Note that the map shows the intensity in logarithmic units. High-latitude intensity fluctuations are generally sub-dominant compared to the Galactic plane emission.

A simple estimate of the overall diffuse flux around the Galactic plane can be derived from a simple density scaling  $n \simeq \exp(-|z|/0.1 \text{ kpc}) \text{ cm}^{-3}$  with distance  $z$  from the Galactic plane and the corresponding integrated column density along the line-of-sight. The result is shown in Figure 14 as a red solid line, where we averaged the diffuse emission over latitudes  $|b| < 2^\circ$ . For the calculation we use Equation (4) with the locally observed CR nucleon flux derived from the model of [132]. This estimate agrees well with more elaborate studies using numerical CR propagation codes to evaluate the CR density across the Galaxy and using non-azimuthal target gas maps [129].

Figure 14 also shows the diffuse flux of cosmic neutrinos observed by IceCube [44]. This indicates that the diffuse flux close to the Galactic plane can dominate over the isotropic diffuse emission observed with IceCube for  $E_\nu \leq 10 \text{ TeV}$ . However, it is unlikely that this Galactic contribution has a strong impact on the interpretation of the IceCube data [129, 134, 135, 136].

Note that the previous estimate is based on the assumption that one can approximate the average Galactic CR density by the local CR flux. This

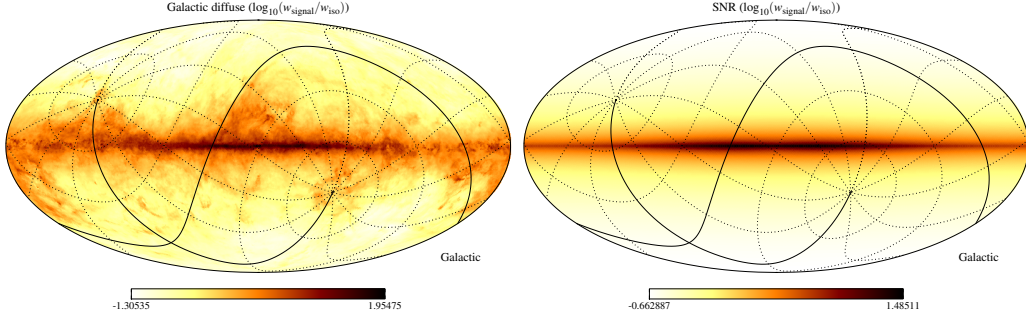


Figure 13: Mollweide projections of expected diffuse Galactic neutrino emission [129]. The left plot shows diffuse emission from CR propagation ( $E_\nu = 10$  TeV) and the right plot the combined emission from supernovae remnants [133]. The mesh indicates the equatorial coordinate system with right ascension  $\alpha = 0^\circ$  and declination  $\delta = 0^\circ$  indicated as solid lines. The color reflects the logarithm of the intensity ratio between the Galactic and an isotropic signal.

is not necessarily the case with more general scenarios introducing spatial density fluctuation, e.g., by accounting for anisotropic diffusion [137], by inhomogeneous diffusion [128], or by strongly inhomogeneous source distributions [138, 139]. Alternatively, a time-dependent local CR injection episode could be responsible for local CR spectra that are softer than the Galactic average [140] and could also lead to an increase of the overall Galactic diffuse emission.

At present, there are various dedicated IceCube analyses that are searching for Galactic diffuse neutrino emission, accounting for uncertainties of morphology and emission spectrum. The simplest test for a signal from the Galactic diffuse emission in the IceCube data is by checking for spatial correlations with the Galactic plane. No significant correlation of events with the Galactic plane was found in four years of high-energy starting event (HESE) data [37]. When letting the Galactic plane size float freely, the best fit returned a value of  $|b| \leq 7.5^\circ$  with a post-trial chance probability of 3.3%. The recent analysis [129] based on 3 years of HESE data [36] showed that even with the poor angular resolution of cascade events the anisotropy produced by a strong Galactic diffuse flux should be visible in data. The upper limit on the contribution to the high-energy data with deposited energy above 60 TeV is about 50%. This is in contrast to the claim of [141] that the 4-year

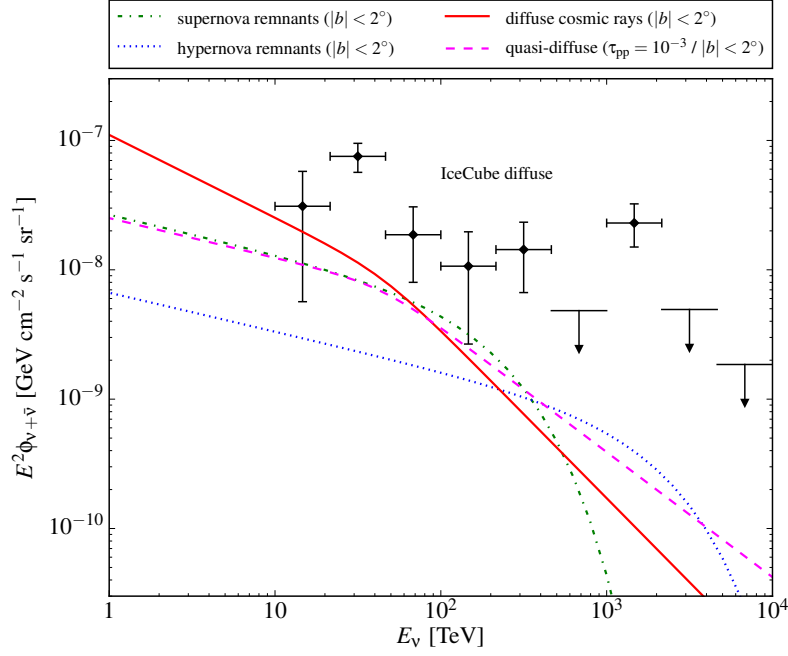


Figure 14: Diffuse emission from the Galactic plane ( $|b| \leq 2^\circ$ ) in comparison to the isotropic diffuse neutrino flux (per flavor) observed by IceCube [44]. We summarize here the Galactic diffuse flux (4), the quasi-diffuse flux (6) from weak Galactic sources (optical thickness  $\tau_{pp} \simeq 10^{-3}$  and diffusion index  $\delta = 1/3$ ), and the quasi-diffuse flux (5) of supernovae and hypernovae ( $\Gamma = 2.3$ ).

HESE update shows evidence of Galactic emission within latitudes  $|b| \leq 10^\circ$  above 100 TeV. In addition, the angular distribution of the muon neutrino data from the recent analysis [42] does not seem to support this claim.

While individual Galactic neutrino sources have not been identified, the cumulative contribution of Galactic sources below the IceCube detection threshold [142] might be identified as extended emission concentrated along the Galactic plane. In general, if  $N_N$  is the (time-integrated) CR nucleon spectrum of a single source, we can define the Galactic neutrino emission from interactions of CRs with ambient gas as

$$E_\nu^2 Q_\nu(E_\nu) \simeq \frac{1}{6} c n \kappa \sigma_{pp} \rho_{\text{act}} [E_N^2 N_N(E_N)]_{E_N=20E_\nu}, \quad (5)$$

where  $n$  is the ambient gas density and  $\rho_{\text{act}}$  is the number density of *active* sources in the Galaxy.

We consider now the case of neutrino emission from supernova remnants (SNR) in our Milky Way following the distribution of Ref. [133]. Similar to the diffuse emission from CR propagation, the intensity distribution of events is concentrated along the Galactic plane as shown in the right plot of Fig. 13. The number of active SNRs can be estimated from the SN rate and the time-scale of the onset of the snow-plow phase which marks the end of the adiabatic Sedov–Taylor phase [143]. From this, one can estimate that a few thousand SNRs are CR emitters at any given time. The maximal energy can be estimated from the ambient gas density, ejecta mass, and velocity to reach  $E_{\text{max,p}} \simeq 5$  PeV. An order of magnitude higher CR energies might be reached in very energetic SNe ( $\simeq 10^{52}$  erg), so-called *hypernovae*, but they are much less frequent than normal SNe with only 1% - 2% of the SNe rate [144, 134].

Figure 14 summarizes the estimated flux of SNRs (green dashed-dotted line) and hypernova remnants (blue dotted line) assuming a source spectral index  $\Gamma \simeq 2.3$  (see Ref. [134] for details). While the source emission spectrum is subdominant at lower energies it is expected to become more important at higher energies because of its harder emission spectrum. In fact, for the choice of parameters in our example, the combined emission of sources becomes comparable to the diffuse emission at energies of 100 TeV, corresponding to neutrinos produced by CRs close to the knee region.

Note that the previous estimate applies more generally than to the case in which SNR are the main sources of Galactic CRs. If we focus on the sources of Galactic CRs, we can relate the (per flavor) neutrino emission rate to that of the CR nucleons as

$$E_\nu^2 Q_\nu(E_\nu) \simeq \frac{1}{6} \kappa \tau_{pp} [E_N^2 Q_N(E_N)]_{E_N=20E_\nu} , \quad (6)$$

where  $\tau_{pp} \ll 1$  is the optical thickness of the source environment for CR-gas interactions, before CRs are released into the Galactic medium. The nucleon emission rate  $Q_N$  is now fixed to the observed CR spectrum by the steady-state solution of the CR diffusion equation. For an active emission period lasting over a time  $t_{\text{act}}$  and an ambient average gas density  $n_{\text{gas}}$ , one can estimate the optical thickness as  $\tau_{pp} \simeq c t_{\text{act}} n_{\text{gas}} \sigma_{pp}$ . For the case of SNRs we can estimate  $t_{\text{act}}$  by the dynamical time-scale  $10^4$  yr (the end of the adiabatic Sedov–Taylor phase [143]) and  $n_{\text{gas}} \simeq 1 \text{ cm}^{-3}$  yielding  $\tau_{pp} \simeq 3 \times 10^{-4}$ . This flux is also shown in Figure 14 as a magenta dashed line assuming  $\tau_{pp} \simeq 10^{-3}$  and a diffusion index  $\delta = 1/3$ . Not surprisingly, this is consistent with our previous estimates of the combined flux of supernova and hypernova

remnants.

The combined neutrino emission of Galactic sources has been studied by various authors [142, 134, 145]. Analogous to the diffuse emission from CR propagation, the contribution of weak Galactic sources can be constrained in the simplest case by the absence of anisotropies. For instance, Ref. [129] argues that a Galactic emission following the distributions of supernova remnants [133] or pulsars [146] can not contribute more than 65% to the HESE three-year data [129]. Even stronger limits can be expected if also the emission spectrum is taken into account.

## **7. Measurements of the local cosmic-ray spectrum and composition**

From the point of view of CR physics, IceCube is a three-dimensional air shower array. The aperture for trajectories that pass through IceTop and within the deep array at its mid-plane is  $\approx 0.25 \text{ km}^2\text{sr}$ , which corresponds to  $\approx 1000$  events per year above 100 PeV, but only a few per year above one EeV. Such coincident events provide information about the primary composition from the ratio of the energy in the muon bundle in the deep ice to the total shower size at the surface. The measurement of the primary spectrum can be extended to the EeV range by using events over a larger angular range reconstructed with only the surface array [147]. Muon bundles reconstructed over a large range of zenith angles with the deep array of IceCube extend the acceptance into the EeV range and provide complementary information to the surface array [148]. IceCube can resolve muons in the deep array laterally separated from the main core by more than the string spacing. The separation distribution measured out to 400 meters shows the concave shape expected from the transition from an exponential to a power-law for the transverse momentum distribution of the parent mesons [149]. Perturbative QCD can be used to calculate the rate of high  $p_T$  muons that reach the detector at large separation. Since production of mesons at high  $p_T$  depends on energy per nucleon, measurement of laterally separated muons is in principle sensitive to primary composition.

Several aspects of IceTop lead to its good energy resolution and its ability to distinguish features in the energy spectrum. The array is at a high altitude so that events are observed closer to shower maximum. As a consequence, fluctuations from event to event are less severe than in an array near sea level. The ice Cherenkov tanks are approximately two radiation lengths deep so



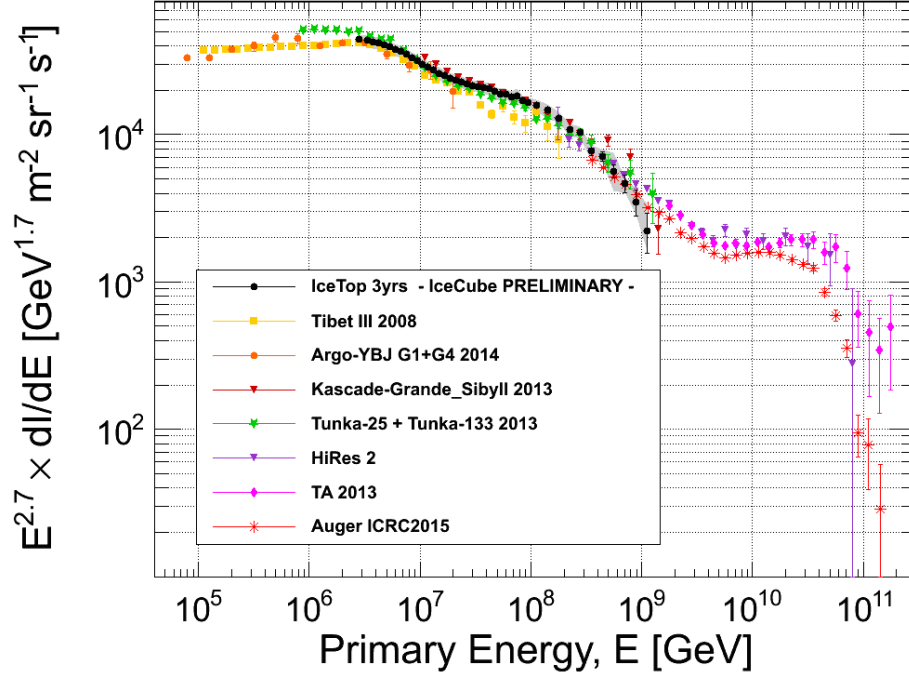


Figure 15: A summary of the primary CR spectrum measured by selected air shower experiments. [150, 151, 152, 153, 154, 155, 156] Measurement from three years of data in IceCube [157] are shown by the black squares.

that the dominant photon component of the surface shower is counted as well as the charged leptons. In contrast, most photons pass through scintillators without converting. The IceTop results are shown by the black points in the compilation of air-shower data in Figure 15. In addition to the knee above 3 PeV, there is a significant hardening of the spectrum around 20 PeV, and the second knee is visible above 200 PeV.

IceCube is the only air shower array currently in operation that can detect TeV muons in the shower core in coincidence with the main shower at the surface. It has much larger acceptance than its predecessors, EASTOP-MACRO [158] and SPASE-AMANDA [159]. Preliminary analysis of the coincidence data in IceCube shows the composition becoming increasingly heavy through the knee region to 100 PeV and beyond [157], although the results become statistically limited at the highest energies.

The increasing fraction of heavy primaries is expected if the knee is the result of Galactic CR accelerators reaching their upper limit. Air shower

experiments make calorimetric measurements of the total energy per particle. Since acceleration and propagation of CRs are both determined by magnetic fields, features in the spectrum should instead depend on magnetic rigidity [160]. Thus, for example, if the characteristic maximum energy for protons is 4 PeV, there should be a corresponding steepening for iron nuclei around 100 PeV total energy. Several air-shower measurements, as reviewed in [161], show the composition changing back toward a lighter composition above 100 PeV as might be expected with the onset of an extra-galactic component at higher energy. The IceCube coincidence analysis gives composition results that agree well with  $\langle \ln(A) \rangle$  measurements summarized in Ref. [161] up to 100 PeV, but the mass value remains high above that energy in some tension with the other data (see Figure 8 in [162]).

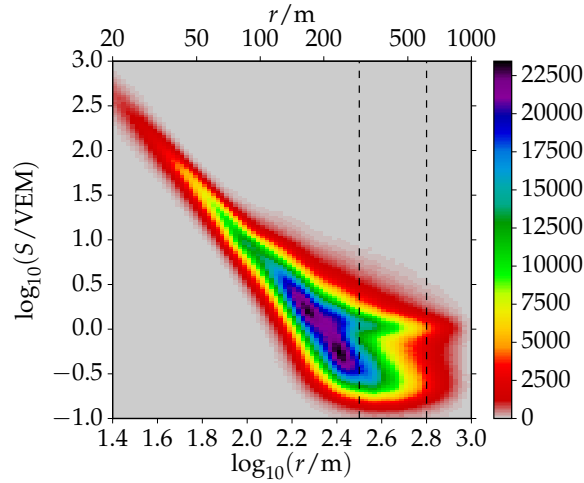


Figure 16: Two-dimensional distribution of signals in showers with primary energies of  $\approx 3$  PeV and zenith angles around  $13^\circ$  as a function of signal in VEM and reconstructed core distance. The horizontal dashed lines indicate the distances at which muon densities as a function of primary energy have been reported [163].

Muons produce a characteristic signal in IceTop tanks because they generate a charge proportional to the length of their tracks. In addition, as the main electromagnetic part of the signal falls off at large distance from the shower core, muons become increasingly prominent, as indicated by the “thumb” centered near one Vertical Equivalent Muon (VEM) in Figure 16. This leads to the possibility of measuring the contribution of  $\sim$  GeV muons

to the showers at the surface [163]. Such a measure of the fraction of muons at the surface opens the possibility of utilizing a different quantity that is sensitive to primary composition. Information from the low energy muons at the surface is complementary to the TeV muons in the shower cores in the coincident event analysis. The comparison, which is ongoing, is of particular interest in light of the fact that different hadronic interaction models show a different behavior for the ratio of GeV to TeV muons. In addition, there are indications that all the standard event generators for  $>\text{EeV}$  air showers produce fewer muons at the surface than observed [164, 165].

Because muons are rare in cascades initiated by photons, the muon content can also be used to reduce the CR background in a search for  $\sim \text{PeV}$   $\gamma$ -rays. A shower reconstructed at the surface with a trajectory that passes through the deep array of IceCube without leaving a signal is a  $\gamma$ -ray candidate. Because of energy losses in the CMB, only Galactic sources would be visible in PeV photons. Using one year of data taken when IceCube was partially complete with 40 strings, a limit on  $\gamma$  rays of several PeV from the Galactic plane was set [166]. Because of the small zenith angle required for events to pass through both components of IceCube, the search was limited to Southern declinations  $< -60^\circ$ . Therefore the analysis covers a limited region of the Galactic plane,  $-80^\circ < \ell < -30^\circ$  in longitude and  $-10^\circ < b < 5^\circ$  in latitude. The sensitivity with five years of data from the full IceCube detector is estimated in this region to be comparable to expectations from some known TeV  $\gamma$ -ray sources if their spectra continue to PeV energies without steepening. An analysis with the completed IceCube detector is underway. Including muon information from the surface detector will allow a larger region of the sky to be explored.

Another search for Galactic CR sources looks for neutrons [167], which would show up as point sources of air showers above the smooth background of charged CRs. No such excesses are identified in 4 years of IceTop data. Limits are placed on potential accelerators of CR protons and nuclei, including millisecond pulsars and high-mass x-ray binaries, by using events with energy  $> 100 \text{ PeV}$  for which the mean distance a neutron would travel before decaying is 100 kpc. Assuming an  $E^{-2}$  spectrum, the limits are of the same order of magnitude in energy flux as might be expected for sources that produce photons in association with acceleration of nuclei that fragment in or near their sources to produce neutrons.

## 8. Anisotropy of local cosmic rays

Through measurement of the energy spectrum and composition of the CR flux, we hope to gain a better understanding of CR sources and acceleration mechanisms. Another quantity accessible to experimental measurement is the arrival direction of the CR particles. In principle, the sky map of CR arrival directions should give us the most direct indication of where the sources might be located. Below several PeV, the sources of CRs are Galactic and the arrival direction distribution should show a correlation with the Galactic plane. However, unlike  $\gamma$  rays and neutrinos, CR particles are charged and therefore repeatedly scattered in the chaotic interstellar magnetic fields. Their arrival direction distribution at Earth is highly isotropic, although a small residual dipole anisotropy is expected from diffusion theory.

Observations made over the last few decades with various surface and underground detectors, together covering an energy range from tens of GeV to tens of PeV, have indeed provided statistically significant evidence for a faint anisotropy in the CR arrival direction distribution [12, 13, 14, 15, 16, 17, 168, 169, 170, 171, 172, 173, 174]. The anisotropy is small, with an amplitude on the order of  $10^{-3}$ , and it shows a strong dependence on energy [17, 174, 175, 176]. It is, however, not well described by a simple dipole. A quantitative description of the anisotropy as a superposition of spherical harmonics [174, 177] shows that while most of the power is in the low-multipole ( $\ell \leq 4$ ) terms, i.e. in the dipole, quadrupole, and octupole terms, features with smaller angular scale down to sizes of a few degrees are also present. These small-scale features have been observed in the TeV range by several experiments [170, 172, 174, 177, 178, 179], and their relative intensity is on the order of  $10^{-5} - 10^{-4}$ . Given the complex nature of the anisotropy, its range from large to small angular scales, and its strong dependence on energy, it has become clear that there is no single process that can account for all observations. Rather, multiple phenomena likely contribute to the anisotropy.

Before IceCube, high-statistics measurements of the CR anisotropy in the TeV energy range were only available from experiments in the Northern Hemisphere. Over the last few years, IceCube has accumulated one of the largest CR data sets at TeV to PeV energies, and a detailed study of the morphology, energy dependence, and stability of the anisotropy over time is possible for the southern sky.

CRs can be studied with IceCube in two independent ways. The in-ice component of IceCube detects downward-going muons created in extensive

air showers caused by CR entering the atmosphere above the detector. Simulations show that the detected muon events are generated by primary CR particles with median energy of about 20 TeV. The trigger rate ranges between 2.5 kHz and 2.9 kHz, with the modulation caused by seasonal variations of the stratospheric temperature and density [180, 181, 182].

The anisotropy can also be studied using the CR air showers detected by IceTop. Its surface location near the shower maximum makes it sensitive to the full electromagnetic component of the shower, not just the muonic component. The detection rate is approximately 30 Hz and the minimum primary particle energy threshold is about 300 TeV. Requiring a minimum of eight IceTop stations leads to a median energy of 1.6 PeV. The IceTop data set therefore provides an independent measurement at PeV energies, close to the knee of the CR spectrum.

A recent study of the CR anisotropy in IceCube and IceTop [174] is based on six years of data taken between May 2009 and May 2015. The data set contains 318 billion CR events observed by IceCube and 172 million events observed with IceTop at higher energies. In order to study the energy dependence of the anisotropy, the IceCube data set is split into nine bins of increasing median energy, ranging from TeV to PeV. The resolution of this energy assignment depends on the detector configuration and energy band but is on the order of 0.5 in  $\log_{10}(E/\text{GeV})$ . It is primarily limited by the relatively large fluctuations in the fraction of the total shower energy that is transferred to the muon bundle.

The most prominent anisotropy observed in the IceCube data at energies below 50 TeV is characterized by a large excess from  $30^\circ$  to  $120^\circ$  in right ascension and a deficit from  $150^\circ$  to  $250^\circ$ . The relative intensity of the anisotropy is at the  $10^{-3}$  level. This large-scale structure that dominates the sky map at lower energies gradually disappears above 50 TeV. Above 100 TeV, a change in the morphology is observed. At higher energies, the anisotropy is characterized by a wide relative deficit from  $30^\circ$  to  $120^\circ$ , with an amplitude increasing with energy up to at least 5 PeV, the highest energies currently accessible to IceCube. The IceTop map at 1.6 PeV shows the same morphology as the IceCube maps at comparable energies. To illustrate this change of the phase of the large-scale anisotropy between TeV and PeV energies, Figure 17 shows the IceCube map at a median energy of 13 TeV (top) to the IceTop map at 1.6 PeV (bottom).

Figure 18 shows the phase (top) and amplitude (bottom) of the dipole component as a function of energy. Since the data are not well described by

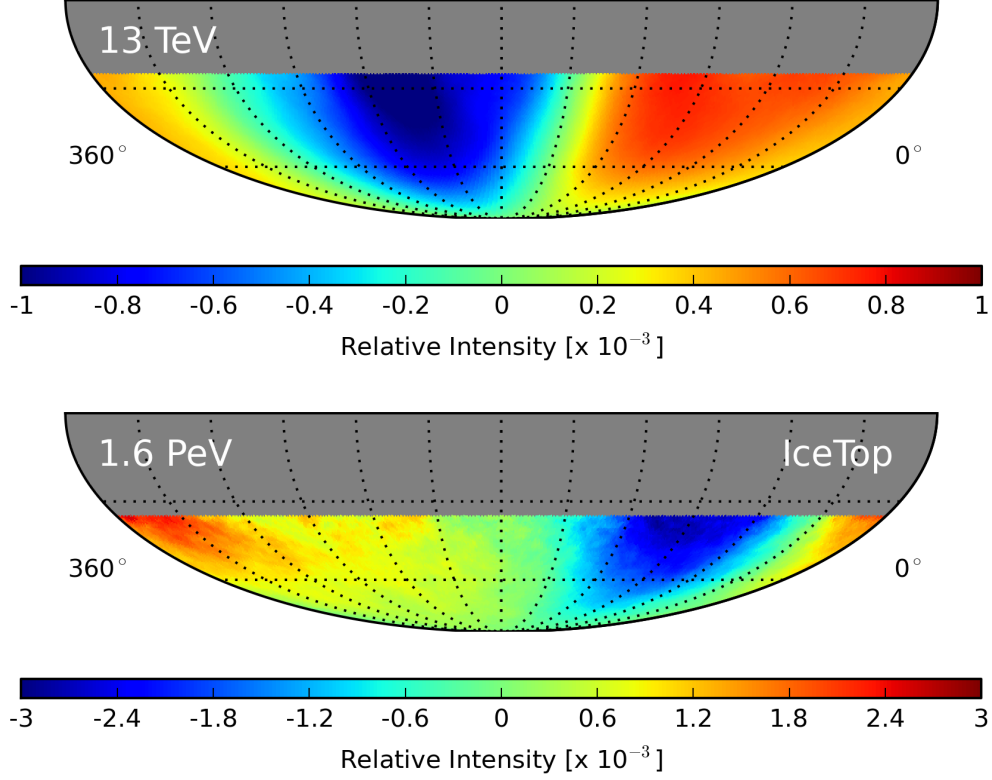


Figure 17: Maps of the relative intensity of CRs in equatorial coordinates for a median energy of 13 TeV (top) and 1.6 PeV (bottom) [174]. The low-energy map is based on IceCube data, the high-energy map on IceTop data. Maps have been smoothed with a  $20^\circ$  smoothing radius.

a dipole, the actual fit is performed including higher-order multipoles, but only the amplitude and phase of the dipole are reported here. The phase shift in the dipole component of the large-scale anisotropy occurs rather rapidly between 100 TeV and 200 TeV. The amplitude of the dipole component rises with energy up to about 10 TeV. Above this energy, it slowly decreases until it has essentially dropped by an order of magnitude at around 200 TeV. It then increases again, with a different phase, up to the highest detected energies. The figure also shows the results from several other experiments in the Northern Hemisphere. The results are generally in good agreement. The difference in the amplitude measured by IceCube and IceTop above 1 PeV is likely due to a difference in the chemical composition of the two data sets. At

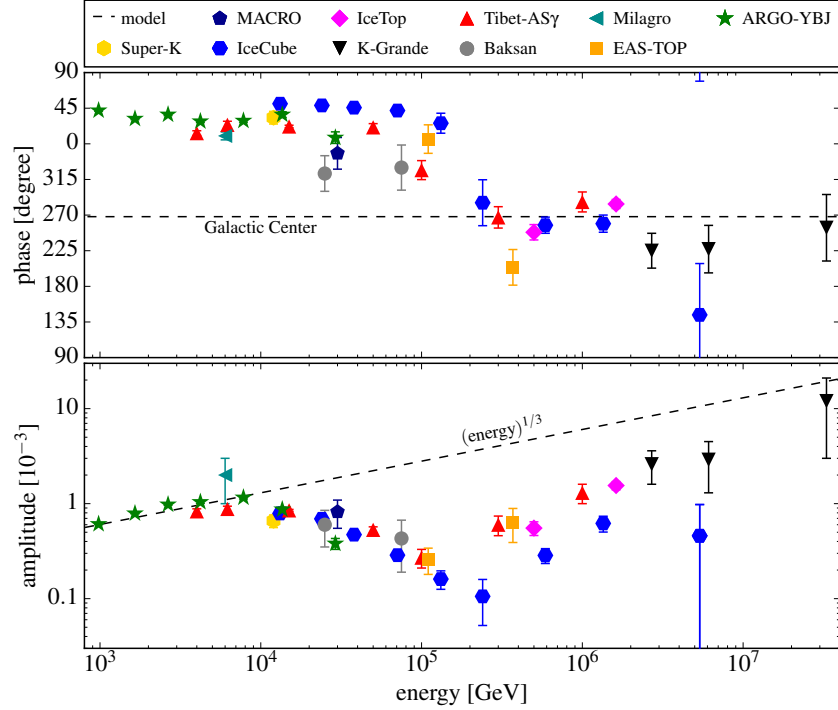


Figure 18: Phase (top) and amplitude (bottom) of the dipole moment of the CR relative intensity map as a function of energy for IceCube (blue), IceTop (pink), and other experiments. Taken from [183].

this energy, the IceTop data set has on average a lighter composition than the IceCube data set because IceTop is not yet fully sensitive to heavier nuclei.

Measurements of a dipole amplitude and phase of the CR flux have also been performed at even higher energies, although the small event rate makes these measurements increasingly difficult. Nevertheless, the Pierre Auger Observatory found that a shift in the phase of the anisotropy occurs again at EeV energies [184]. Below 1 EeV, the dipole phase is consistent with the phase observed by IceCube at PeV energies. Around 4 EeV, the phase changes and the relative excess moves towards the range in right ascension that includes the Galactic anti-center direction. In between the IceCube and Pierre Auger measurements, KASCADE-Grande data shows a dipole phase between median energies of 2.7 PeV and 33 PeV [185], which is consistent with the IceCube results at PeV energies.

While the large-scale structure dominates the anisotropy, there is also

anisotropy on smaller scales. The small-scale structure, with a relative intensity on the order of  $10^{-4}$ , and therefore roughly one order of magnitude weaker, becomes visible after the best-fit dipole and quadrupole are subtracted from the sky map. Figure 19 shows the relative intensity of the residual map. Several excess and deficit regions are visible at angular scales approaching the angular resolution of IceCube for CR primaries. The strongest of these regions have statistical significances exceeding  $10\sigma$ .

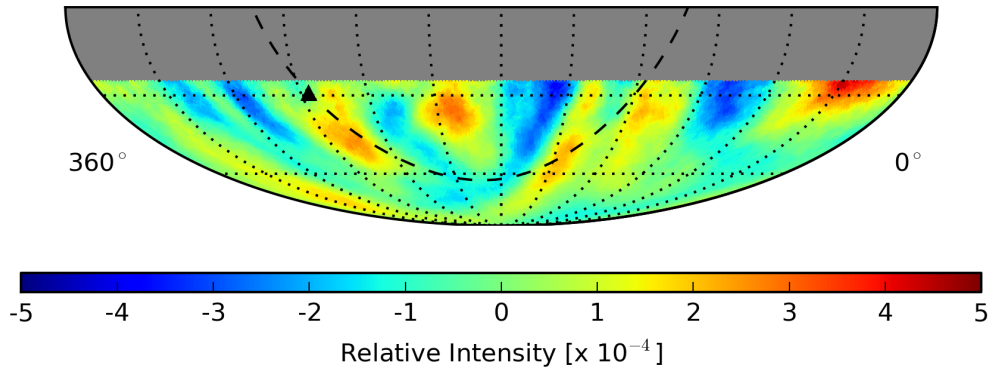


Figure 19: Relative intensity map of the full 6-year IceCube data set [174] for all energies (median energy 20 TeV) after dipole- and quadrupole-subtraction. The subtraction of the dominant low-order multipoles reveals the small-scale structure with a relative intensity of order  $10^{-4}$ . The dashed line indicates the Galactic plane and the triangle indicates the Galactic center.

A study of the time dependence of the large- and small-scale structure over the six-year period covered by this analysis reveals no significant change with time. An analysis of data taken with the AMANDA detector between 2000 and 2006 also did not find any significant time variation of the observed large-scale anisotropy [186].

The source of the CR anisotropy remains unknown. Homogeneous and isotropic diffusive propagation of CRs in the Galaxy from discrete sources leads to a density gradient of CRs, which produces a dipole. While a small residual dipole anisotropy is therefore expected from diffusion theory, the observed anisotropy has a considerably more complex morphology than simple diffusion models suggest. To explain the formation of the non-dipolar structures, additional processes like non-diffusive propagation of CRs in perturbed magnetic fields need to be considered.



To complicate matters further, the observed amplitude of the anisotropy is smaller than predicted from diffusion theory. Numerical studies show that particular realizations of Galactic source distributions reproduce the observed energy dependence of the anisotropy [187], but simulations based on plausible source distributions typically predict a larger amplitude for the anisotropy than what is observed [187, 188, 189, 190, 191]. The misalignment between the direction of the CR density gradient and the interstellar magnetic field lines may explain the smaller observed amplitude component (see [192, 193]).

Non-dipolar structures may be produced by the interactions of CRs with an isotropically turbulent interstellar magnetic field. Scattering processes with stochastic magnetic instabilities produce perturbations in the arrival directions within the scattering mean free path. Such perturbations may be observed as stochastic localized excess or deficit regions [194, 195, 196, 197, 198, 199, 200].

It has been shown recently that one or more local sources at Galactic longitudes between  $120^\circ$  and  $300^\circ$  in the presence of a strong ordered magnetic field in our local environment can explain the observations [201]. The Vela SNR, created about 12,000 years ago, is identified as a candidate local source. The discrepancy between the predicted and observed amplitude could, at least in part, be a result of the limited capabilities of ground-based detectors to reconstruct the true underlying anisotropy. New analysis methods to correct for some of these observational biases have recently been developed [202].

There are other sources of magnetic perturbations on smaller scales, for example the heliosphere, formed by the interaction between the solar wind and the interstellar flow. The heliosphere constitutes a perturbation in the  $3\mu\text{G}$  local interstellar magnetic field. The local magnetic field draping around the heliosphere might be a significant source of resonant scattering, capable of redistributing the arrival directions of TeV CR particles [203, 204, 205, 206]. CR acceleration from magnetic reconnection in the heliotail has also been proposed as an explanation of the localized small-scale excess regions and their harder spectrum [207, 208].

## 9. Conclusions

We have reviewed how observations of neutrinos and cosmic rays with the IceCube neutrino telescope and its surface array IceTop have impacted our knowledge about the high-energy non-thermal universe. Only three years

after their first detection, we know the spectrum and flavor composition of cosmic neutrinos in the energy interval between 10 TeV and several PeV with encouraging precision. The distribution of the neutrinos on the sky is compatible with an isotropic distribution, excluding a purely Galactic origin.

Surprisingly, no individual neutrino sources or transients have been observed so far that would pinpoint the origin of the cosmic neutrinos. However, putting all the information together, we can already make important statements about their origin. Blazar jets and GRBs can only be responsible for small fractions of the observed cosmic neutrinos. Less luminous sources with higher number densities are needed to explain the observed level of astrophysical neutrinos and the absence of detectable point sources at the same time. Coincidences of neutrino events with transient phenomena, a SN explosion and a Blazar flare, have been observed, however the circumstances make it impossible to exclude a chance occurrence. No neutrinos have been observed thus far that could be attributed to the GZK effect. Again, the non-observation of associated neutrinos starts to constrain evolution scenarios for UHE CR sources.

Direct observations of the spectrum and the anisotropy of CRs at TeV and PeV energies with IceCube and IceTop have provided accurate measurements of the shape of the CR spectrum from few PeV to above one EeV. Searches for point sources of photons or neutrons among the CR air showers recorded have been negative so far. Additionally, the large statistics of CR air showers collected by IceCube has allowed the most precise measurement of the CR anisotropy in the Southern hemisphere, confirming and extending the measurements from the Northern hemisphere. Both large-scale and small-scale components have been detected, however their origin is still not well understood.

Both IceCube and IceTop continue to collect data, likely for at least another decade. As the statistics of cosmic neutrinos and CRs increases, and the understanding of systematic effects improves, we can expect significant advances in understanding the neutrino sky, the origin of CRs, and their propagation and arrival at Earth. However, the prospects for what IceCube can achieve within a reasonable time span of a few decades are limited by its size. Based on the experience and success of IceCube, efforts are underway to develop a next generation instrument, IceCube-Gen2 [209]. With its five times better sensitivity for sources than IceCube, ten times the statistics for cosmic neutrinos and at least ten times larger area for a surface array, it will truly mark the next big step towards understanding the origin and

propagation of cosmic rays.

## 10. Acknowledgements

We acknowledge the support from the following agencies: U.S. National Science Foundation - Office of Polar Programs, U.S. National Science Foundation - Physics Division, University of Wisconsin Alumni Research Foundation, the Grid Laboratory Of Wisconsin (GLOW) grid infrastructure at the University of Wisconsin - Madison, the Open Science Grid (OSG) grid infrastructure; U.S. Department of Energy, and National Energy Research Scientific Computing Center, the Louisiana Optical Network Initiative (LONI) grid computing resources; Natural Sciences and Engineering Research Council of Canada, WestGrid and Compute/Calcul Canada; Swedish Research Council, Swedish Polar Research Secretariat, Swedish National Infrastructure for Computing (SNIC), and Knut and Alice Wallenberg Foundation, Sweden; German Ministry for Education and Research (BMBF), Deutsche Forschungsgemeinschaft (DFG), Helmholtz Alliance for Astroparticle Physics (HAP), Research Department of Plasmas with Complex Interactions (Bochum), Germany; Fund for Scientific Research (FNRS-FWO), FWO Odysseus programme, Flanders Institute to encourage scientific and technological research in industry (IWT), Belgian Federal Science Policy Office (Belspo); University of Oxford, United Kingdom; Marsden Fund, New Zealand; Australian Research Council; Japan Society for Promotion of Science (JSPS); the Swiss National Science Foundation (SNSF), Switzerland; National Research Foundation of Korea (NRF); Villum Fonden, Danish National Research Foundation (DNRF), Denmark

## References

- [1] M. G. Aartsen, et al., Evidence for High-Energy Extraterrestrial Neutrinos at the IceCube Detector, *Science* 342 (2013) 1242856.
- [2] A. M. Hillas, The Origin of Ultra-High-Energy Cosmic Rays, *Ann. Rev. Astron. Astrophys.* 22 (1984) 425–444.
- [3] E. Waxman, J. N. Bahcall, High-energy neutrinos from cosmological gamma-ray burst fireballs, *Phys. Rev. Lett.* 78 (1997) 2292–2295.
- [4] K. Fang, K. Kotera, A. V. Olinto, Newly-born pulsars as sources of ultrahigh energy cosmic rays, *Astrophys. J.* 750 (2012) 118.
- [5] K. Mannheim, The proton blazar, *Astronomy and Astrophysics* 269 (1993) 67–76.
- [6] F. W. Stecker, C. Done, M. H. Salamon, P. Sommers, High-energy neutrinos from active galactic nuclei, *Phys. Rev. Lett.* 66 (1991) 2697–2700.
- [7] K. Kashiyama, P. Mészáros, Galaxy Mergers as a Source of Cosmic Rays, Neutrinos, and Gamma Rays, *Astrophys. J. Lett.* 790 (2014) L14.
- [8] M. Ahlers, et al. (2010). FERMILAB-FN-0847-A, YITP-SB-10-01.
- [9] K. Greisen, End to the cosmic ray spectrum?, *Phys. Rev. Lett.* 16 (1966) 748–750.
- [10] G. T. Zatsepin, V. A. Kuzmin, Upper limit of the spectrum of cosmic rays, *JETP Lett.* 4 (1966) 78–80. [*Pisma Zh. Eksp. Teor. Fiz.* 4,114(1966)].
- [11] K. A. Olive, Review of Particle Physics, *Chin. Phys.* C40 (2016) 100001.
- [12] M. Amenomori, et al., Large-Scale Sidereal Anisotropy of Galactic Cosmic-Ray Intensity Observed by the Tibet Air Shower Array, *Astrophys. J. Lett.* 626 (2005) L29–L32.

- [13] M. Amenomori, et al., Anisotropy and Corotation of Galactic Cosmic Rays, *Science* 314 (2006) 439–443.
- [14] G. Guillian, et al., Observation of the anisotropy of 10 TeV primary cosmic ray nuclei flux with the Super-Kamiokande-I detector, *Phys. Rev. D* 75 (2007) 062003.
- [15] A. Abdo, et al., The Large-Scale Cosmic-Ray Anisotropy as Observed with Milagro, *Astrophys. J.* 698 (2009) 2121–2130.
- [16] J. De Jong, et al., Observations of Large Scale Sidereal Anisotropy in 1 and 11 TeV cosmic rays from the MINOS experiment. (arXiv:1201.2621), *Proc. 32nd Int. Cosmic Ray Conference, Beijing, China* 4 (2011) 46.
- [17] B. Bartoli, et al., ARGO-YBJ Observation of the Large-scale Cosmic Ray Anisotropy During the Solar Minimum between Cycles 23 and 24, *Astrophys. J.* 809 (2015) 90.
- [18] I. A. Belolaptikov, et al., The Baikal underwater neutrino telescope: Design, performance and first results, *Astropart. Phys.* 7 (1997) 263–282.
- [19] M. Ageron, et al., ANTARES: the first undersea neutrino telescope, *Nucl. Instrum. Meth. A* 656 (2011) 11–38.
- [20] S. Adrian-Martinez, et al., Letter of intent for KM3NeT 2.0, *J. Phys. G* 43 (2016) 084001.
- [21] A. D. Avrorin, et al., Sensitivity of the Baikal-GVD neutrino telescope to neutrino emission toward the center of the galactic dark matter halo, *JETP Lett.* 101 (2015) 289–294.
- [22] A. Achterberg, et al., First Year Performance of The IceCube Neutrino Telescope, *Astropart. Phys.* 26 (2006) 155–173.
- [23] R. Abbasi, et al., The IceCube Data Acquisition System: Signal Capture, Digitization, and Timestamping, *Nucl. Instrum. Meth. A* 601 (2009) 294–316.
- [24] M. G. Aartsen, et al., The IceCube Neutrino Observatory: Instrumentation and Online Systems, *arXiv eprints* (2016) astro-ph/1612.05093.

- [25] R. Abbasi, et al., IceTop: The surface component of IceCube, Nucl. Instrum. Meth. A700 (2013) 188–220.
- [26] R. Abbasi, et al., The Design and Performance of IceCube DeepCore, Astropart. Phys. 35 (2012) 615–624.
- [27] J. G. Learned, S. Pakvasa, Detecting tau-neutrino oscillations at PeV energies, Astropart. Phys. 3 (1995) 267–274.
- [28] M. G. Aartsen, et al., Measurement of South Pole ice transparency with the IceCube LED calibration system, Nucl. Instrum. Meth. A711 (2013) 73–89.
- [29] M. G. Aartsen, et al., Energy reconstruction methods in the IceCube neutrino telescope, Journal of Instrumentation 9 (2014) P03009.
- [30] R. Abbasi, et al., A Search for a Diffuse Flux of Astrophysical Muon Neutrinos with the IceCube 40-String Detector, Phys. Rev. D84 (2011) 082001.
- [31] M. G. Aartsen, et al., Development of a General Analysis and Unfolding Scheme and its Application to Measure the Energy Spectrum of Atmospheric Neutrinos with IceCube, Eur. Phys. J. C75 (2015) 116.
- [32] M. G. Aartsen, et al., Measurement of the Atmospheric  $\nu_e$  flux in IceCube, Phys. Rev. Lett. 110 (2013) 151105.
- [33] M. G. Aartsen, et al., Measurement of the Atmospheric  $\nu_e$  Spectrum with IceCube, Phys. Rev. D91 (2015) 122004.
- [34] R. Enberg, M. H. Reno, I. Sarcevic, High energy neutrinos from charm in astrophysical sources, Phys. Rev. D79 (2009) 053006.
- [35] M. G. Aartsen, et al., First observation of PeV-energy neutrinos with IceCube, Phys. Rev. Lett. 111 (2013) 021103.
- [36] M. G. Aartsen, et al., Observation of High-Energy Astrophysical Neutrinos in Three Years of IceCube Data, Phys. Rev. Lett. 113 (2014) 101101.

- [37] M. G. Aartsen, et al., The IceCube Neutrino Observatory - Contributions to ICRC 2015 Part II: Atmospheric and Astrophysical Diffuse Neutrino Searches of All Flavors, 6: Observation of Astrophysical Neutrinos in four Years of IceCube Data, in: Proceedings, 34th International Cosmic Ray Conference (ICRC 2015): The Hague, The Netherlands, July 30-August 6, 2015 (arXiv:1510.03223).
- [38] M. G. Aartsen, et al., Flavor Ratio of Astrophysical Neutrinos above 35 TeV in IceCube, Phys. Rev. Lett. 114 (2015) 171102.
- [39] M. G. Aartsen, et al., Atmospheric and astrophysical neutrinos above 1 TeV interacting in IceCube, Phys. Rev. D91 (2015) 022001.
- [40] M. G. Aartsen, et al., The IceCube Neutrino Observatory - Contributions to ICRC 2015 Part II: Atmospheric and Astrophysical Diffuse Neutrino Searches of All Flavors, 9: High Energy Astrophysical Neutrino Flux Characteristics for Neutrino-induced Cascades Using IC79 and IC86-String IceCube Configurations, in: Proceedings, 34th International Cosmic Ray Conference (ICRC 2015): The Hague, The Netherlands, July 30-August 6, 2015 (arXiv:1510.05223).
- [41] M. G. Aartsen, et al., Evidence for Astrophysical Muon Neutrinos from the Northern Sky with IceCube, Phys. Rev. Lett. 115 (2015) 081102.
- [42] M. G. Aartsen, et al., Observation and Characterization of a Cosmic Muon Neutrino Flux from the Northern Hemisphere using six years of IceCube data, Astrophys. J. 833 (2016) 3.
- [43] M. G. Aartsen, et al., Search for Astrophysical Tau Neutrinos in Three Years of IceCube Data, Phys. Rev. D93 (2016) 022001.
- [44] M. G. Aartsen, et al., A combined maximum-likelihood analysis of the high-energy astrophysical neutrino flux measured with IceCube, Astrophys. J. 809 (2015) 98.
- [45] M. G. Aartsen, et al., The IceCube Neutrino Observatory - Contributions to ICRC 2015 Part II: Atmospheric and Astrophysical Diffuse Neutrino Searches of All Flavors, 3: Combined Analysis of the High-Energy Cosmic Neutrino Flux at the IceCube Detector, in: Proceedings, 34th International Cosmic Ray Conference (ICRC 2015): The Hague, The Netherlands, July 30-August 6, 2015 (arXiv:1510.05223).

- [46] S. R. Klein, R. E. Mikkelsen, J. Becker Tjus, Muon Acceleration in Cosmic-ray Sources, *Astrophys. J.* 779 (2013) 106.
- [47] M. G. Aartsen, et al., All-sky search for time-integrated neutrino emission from astrophysical sources with 7 years of IceCube data, *arXiv eprints* (2016) astro-ph/1609.04981.
- [48] S. Adrian-Martinez, et al., Searches for Point-like and extended neutrino sources close to the Galactic Centre using the ANTARES neutrino Telescope, *Astrophys. J.* 786 (2014) L5.
- [49] A. Reimer, Photon-neutrino flux correlations from hadronic models of AGN?, *Proceedings, 34th International Cosmic Ray Conference (ICRC 2015)* (2015).
- [50] M. Petropoulou, S. Dimitrakoudis, P. Padovani, A. Mastichiadis, E. Resconi, Photohadronic origin of  $\gamma$ -ray BL Lac emission: implications for IceCube neutrinos, *MNRAS* 448 (2015) 2412–2429.
- [51] M. G. Aartsen, et al., Searches for Time Dependent Neutrino Sources with IceCube Data from 2008 to 2012, *Astrophys. J.* 807 (2015) 46.
- [52] M. G. Aartsen, et al., Searches for Extended and Point-like Neutrino Sources with Four Years of IceCube Data, *Astrophys. J.* 796 (2014) 109.
- [53] M. G. Aartsen, et al., Search for Time-independent Neutrino Emission from Astrophysical Sources with 3 yr of IceCube Data, *Astrophys. J.* 779 (2013) 132.
- [54] R. Abbasi, et al., Time-Dependent Searches for Point Sources of Neutrinos with the 40-String and 22-String Configurations of IceCube, *Astrophys. J.* 744 (2012) 1.
- [55] S. Adrian-Martinez, et al., Search for Cosmic Neutrino Point Sources with Four Year Data of the ANTARES Telescope, *Astrophys. J.* 760 (2012) 53.
- [56] R. Abbasi, et al., An absence of neutrinos associated with cosmic-ray acceleration in  $\gamma$ -ray bursts, *Nature* 484 (2012) 351–353.



- [57] S. Adrian-Martinez, et al., Search for muon neutrinos from gamma-ray bursts with the ANTARES neutrino telescope using 2008 to 2011 data, *Astron. Astrophys.* 559 (2013) A9.
- [58] P. Lipari, Perspectives of High Energy Neutrino Astronomy, *Nucl. Instrum. Meth.* A567 (2006) 405–417.
- [59] J. K. Becker, W. Rhode, P. L. Biermann, K. Muenich, Astrophysical implications of high energy neutrino limits. 1. Overall diffuse limits, *Astropart. Phys.* 28 (2008) 98–118.
- [60] A. Silvestri, S. W. Barwick, Constraints on Extragalactic Point Source Flux from Diffuse Neutrino Limits, *Phys. Rev.* D81 (2010) 023001.
- [61] M. Ahlers, F. Halzen, Pinpointing Extragalactic Neutrino Sources in Light of Recent IceCube Observations, *Phys. Rev.* D90 (2014) 043005.
- [62] A. M. Hopkins, J. F. Beacom, On the normalisation of the cosmic star formation history, *Astrophys. J.* 651 (2006) 142–154.
- [63] H. Yuksel, M. D. Kistler, J. F. Beacom, A. M. Hopkins, Revealing the High-Redshift Star Formation Rate with Gamma-Ray Bursts, *Astrophys. J.* 683 (2008) L5–L8.
- [64] M. G. Aartsen, et al., The contribution of Fermi-2LAC blazars to the diffuse TeV-PeV neutrino flux, *arXiv eprints* (2016) astro-ph/1611.03874.
- [65] V. S. Berezinsky, G. T. Zatsepin, Cosmic rays at ultrahigh-energies (neutrino?), *Phys. Lett.* B28 (1969) 423–424.
- [66] S. Yoshida, M. Teshima, Energy spectrum of ultrahigh-energy cosmic rays with extragalactic origin, *Prog. Theor. Phys.* 89 (1993) 833–845.
- [67] R. J. Protheroe, P. A. Johnson, Propagation of ultrahigh-energy protons over cosmological distances and implications for topological defect models, *Astropart. Phys.* 4 (1996) 253.
- [68] R. Engel, D. Seckel, T. Stanev, Neutrinos from propagation of ultrahigh-energy protons, *Phys. Rev.* D64 (2001) 093010.

- [69] V. Berezhinsky, A. Z. Gazizov, S. I. Grigorieva, On astrophysical solution to ultrahigh-energy cosmic rays, *Phys. Rev. D* 74 (2006) 043005.
- [70] Z. Fodor, S. D. Katz, A. Ringwald, H. Tu, Bounds on the cosmogenic neutrino flux, *JCAP* 0311 (2003) 015.
- [71] H. Yuksel, M. D. Kistler, Enhanced cosmological GRB rates and implications for cosmogenic neutrinos, *Phys. Rev. D* 75 (2007) 083004.
- [72] H. Takami, K. Murase, S. Nagataki, K. Sato, Cosmogenic neutrinos as a probe of the transition from Galactic to extragalactic cosmic rays, *Astropart. Phys.* 31 (2009) 201–211.
- [73] V. Berezhinsky, A. Gazizov, M. Kachelriess, S. Ostapchenko, Restricting UHECRs and cosmogenic neutrinos with Fermi-LAT, *Phys. Lett. B* 695 (2011) 13–18.
- [74] M. Ahlers, L. A. Anchordoqui, M. C. Gonzalez-Garcia, F. Halzen, S. Sarkar, GZK Neutrinos after the Fermi-LAT Diffuse Photon Flux Measurement, *Astropart. Phys.* 34 (2010) 106–115.
- [75] G. B. Gelmini, O. Kalashev, D. V. Semikoz, Gamma-Ray Constraints on Maximum Cosmogenic Neutrino Fluxes and UHECR Source Evolution Models, *JCAP* 1201 (2012) 044.
- [76] G. Decerprit, D. Allard, Constraints on the origin of ultrahigh energy cosmic rays from cosmogenic neutrinos and photons, *Astron. Astrophys.* 535 (2011) A66.
- [77] J. Heinze, D. Boncioli, M. Bustamante, W. Winter, Cosmogenic Neutrinos Challenge the Cosmic Ray Proton Dip Model, *Astrophys. J.* 825 (2016) 122.
- [78] A. D. Supanitsky, Implications of gamma-ray observations on proton models of ultrahigh energy cosmic rays, *Phys. Rev. D* 94 (2016) 063002.
- [79] A. A. Abdo, et al., The Spectrum of the Isotropic Diffuse Gamma-Ray Emission Derived From First-Year Fermi Large Area Telescope Data, *Phys. Rev. Lett.* 104 (2010) 101101.
- [80] M. Ackermann, et al., The spectrum of isotropic diffuse gamma-ray emission between 100 MeV and 820 GeV, *Astrophys. J.* 799 (2015) 86.

- [81] D. Hooper, A. Taylor, S. Sarkar, The Impact of heavy nuclei on the cosmogenic neutrino flux, *Astropart. Phys.* 23 (2005) 11–17.
- [82] M. Ave, N. Busca, A. V. Olinto, A. A. Watson, T. Yamamoto, Cosmogenic neutrinos from ultra-high energy nuclei, *Astropart. Phys.* 23 (2005) 19–29.
- [83] D. Hooper, S. Sarkar, A. M. Taylor, The intergalactic propagation of ultrahigh energy cosmic ray nuclei, *Astropart. Phys.* 27 (2007) 199–212.
- [84] D. Allard, et al., Cosmogenic Neutrinos from the propagation of Ultrahigh Energy Nuclei, *JCAP* 0609 (2006) 005.
- [85] L. A. Anchordoqui, H. Goldberg, D. Hooper, S. Sarkar, A. M. Taylor, Predictions for the Cosmogenic Neutrino Flux in Light of New Data from the Pierre Auger Observatory, *Phys. Rev. D* 76 (2007) 123008.
- [86] R. Aloisio, V. Berezhinsky, A. Gazizov, Ultra High Energy Cosmic Rays: The disappointing model, *Astropart. Phys.* 34 (2011) 620–626.
- [87] K. Kotera, D. Allard, A. V. Olinto, Cosmogenic Neutrinos: parameter space and detectability from PeV to ZeV, *JCAP* 1010 (2010) 013.
- [88] M. Ahlers, J. Salvado, Cosmogenic gamma-rays and the composition of cosmic rays, *Phys. Rev. D* 84 (2011) 085019.
- [89] M. Ahlers, F. Halzen, Minimal Cosmogenic Neutrinos, *Phys. Rev. D* 86 (2012) 083010.
- [90] M. G. Aartsen, et al., Constraints on ultra-high-energy cosmic ray sources from a search for neutrinos above 10 PeV with IceCube, *Phys. Rev. Lett.* 117 (2016) 241101.
- [91] K. Murase, Y. Inoue, C. D. Dermer, Diffuse neutrino intensity from the inner jets of active galactic nuclei: Impacts of external photon fields and the blazar sequence, *Phys. Rev. D* 90 (2014) 023007.
- [92] P. Padovani, M. Petropoulou, P. Giommi, E. Resconi, A simplified view of blazars: the neutrino background, *Mon. Not. Roy. Astron. Soc.* 452 (2015) 1877–1887.

- [93] E. Waxman, Cosmological gamma-ray bursts and the highest energy cosmic rays, *Phys. Rev. Lett.* 75 (1995) 386–389.
- [94] M. G. Aartsen, et al., An All-Sky Search for Three Flavors of Neutrinos from Gamma-Ray Bursts with the IceCube Neutrino Observatory, *Astrophys. J.* 824 (2016) 115.
- [95] M. Ahlers, M. C. Gonzalez-Garcia, F. Halzen, GRBs on probation: testing the UHE CR paradigm with IceCube, *Astropart. Phys.* 35 (2011) 87–94.
- [96] M. Bustamante, P. Baerwald, K. Murase, W. Winter, Neutrino and cosmic-ray emission from multiple internal shocks in gamma-ray bursts, *Nature Commun.* 6 (2015) 6783.
- [97] N. Senno, K. Murase, P. Meszaros, Choked Jets and Low-Luminosity Gamma-Ray Bursts as Hidden Neutrino Sources, *Phys. Rev. D* 93 (2016) 083003.
- [98] S. Razzaque, P. Meszaros, E. Waxman, High energy neutrinos from a slow jet model of core collapse supernovae, *Mod. Phys. Lett. A* 20 (2005) 2351–2368.
- [99] S. Ando, J. F. Beacom, Revealing the supernova-gamma-ray burst connection with TeV neutrinos, *Phys. Rev. Lett.* 95 (2005) 061103.
- [100] I. Tamborra, S. Ando, Inspecting the supernova – gamma-ray-burst connection with high-energy neutrinos, *Phys. Rev. D* 93 (2016) 053010.
- [101] J. Hjorth, J. S. Bloom, The Gamma-Ray Burst - Supernova Connection, volume 51 of *Cambridge Astrophysics Series*, Cambridge University Press, Cambridge, pp. 169–190.
- [102] K. Murase, T. A. Thompson, E. O. Ofek, Probing Cosmic-Ray Ion Acceleration with Radio-Submm and Gamma-Ray Emission from Interaction-Powered Supernovae, *Mon. Not. Roy. Astron. Soc.* 440 (2014) 2528–2543.
- [103] V. N. Zirakashvili, V. S. Ptuskin, Type II<sub>n</sub> supernovae as sources of high energy astrophysical neutrinos, *Astropart. Phys.* 78 (2016) 28–34.

- [104] R. Abbasi, et al., Searching for soft relativistic jets in core-collapse supernovae with the IceCube optical follow-up program, *Astron. Astrophys.* 539 (2012) A60.
- [105] N. M. Law, et al., The Palomar Transient Factory: System Overview, Performance, and First Results, *Publications of the Astronomical Society of the Pacific* 121 (2009) 1395–1408.
- [106] M. G. Aartsen, et al., The Detection of a SN IIn in Optical Follow-up Observations of IceCube Neutrino Events, *Astrophys. J.* 811 (2015) 52.
- [107] S. Smartt, et al., GCN Circular 19381 (2016).
- [108] M. G. Aartsen, et al., Very High-Energy Gamma-Ray Follow-Up Program Using Neutrino Triggers from IceCube, *arXiv eprints* (2016) astro-ph/1610.01814.
- [109] M. Kadler, et al., Coincidence of a high-fluence blazar outburst with a PeV-energy neutrino event, *Nature Phys.* 12 (2016) 807–814.
- [110] M. W. E. Smith, et al., The Astrophysical Multimessenger Observatory Network (AMON), *Astropart. Phys.* 45 (2013) 56–70.
- [111] M. G. Aartsen, et al., The IceCube Realtime Alert System, *arXiv eprints* (2016) astro-ph/1612.06028.
- [112] B. P. Abbott, et al., Observation of Gravitational Waves from a Binary Black Hole Merger, *Physical Review Letters* 116 (2016) 061102.
- [113] S. Adrian-Martinez, et al., High-energy Neutrino follow-up search of Gravitational Wave Event GW150914 with ANTARES and IceCube, *Phys. Rev. D* 93 (2016) 122010.
- [114] W. Baade, F. Zwicky, Cosmic Rays from Super-novae, *Proceedings of the National Academy of Science* 20 (1934) 259–263.
- [115] M. Ackermann, et al., Detection of the Characteristic Pion-Decay Signature in Supernova Remnants, *Science* 339 (2013) 807.
- [116] P. Blasi, The origin of the positron excess in cosmic rays, *Phys. Rev. Lett.* 103 (2009) 051104.

- [117] P. Mertsch, S. Sarkar, AMS-02 data confront acceleration of cosmic ray secondaries in nearby sources, *Phys. Rev. D* **90** (2014) 061301.
- [118] O. Adriani, et al., An anomalous positron abundance in cosmic rays with energies 1.5-100 GeV, *Nature* **458** (2009) 607–609.
- [119] M. Ackermann, et al., Measurement of separate cosmic-ray electron and positron spectra with the Fermi Large Area Telescope, *Phys. Rev. Lett.* **108** (2012) 011103.
- [120] L. Accardo, et al., High Statistics Measurement of the Positron Fraction in Primary Cosmic Rays of 0.5500 GeV with the Alpha Magnetic Spectrometer on the International Space Station, *Phys. Rev. Lett.* **113** (2014) 121101.
- [121] M. Ahlers, P. Mertsch, S. Sarkar, On cosmic ray acceleration in supernova remnants and the FERMI/PAMELA data, *Phys. Rev. D* **80** (2009) 123017.
- [122] F. W. Stecker, Diffuse Fluxes of Cosmic High-Energy Neutrinos, *Astrophys. J.* **228** (1979) 919–927.
- [123] G. Domokos, B. Elliott, S. Kovesi-Domokos, Cosmic neutrino production in the Milky Way, *J. Phys. G* **19** (1993) 899–912.
- [124] V. S. Berezinsky, T. K. Gaisser, F. Halzen, T. Stanev, Diffuse radiation from cosmic ray interactions in the galaxy, *Astropart. Phys.* **1** (1993) 281–288.
- [125] D. L. Bertsch, et al., Diffuse Gamma-Ray Emission in the Galactic Plane from Cosmic-Ray, Matter, and Photon Interactions, *Astrophys. J.* **416** (1993) 587.
- [126] G. Ingelman, M. Thunman, Particle production in the interstellar medium, *arXiv eprints* (1996) hep-ph/9604286.
- [127] C. Evoli, D. Grasso, L. Maccione, Diffuse Neutrino and Gamma-ray Emissions of the Galaxy above the TeV, *JCAP* **0706** (2007) 003.
- [128] D. Gaggero, D. Grasso, A. Marinelli, A. Urbano, M. Valli, The gamma-ray and neutrino sky: A consistent picture of Fermi-LAT, Milagro, and IceCube results, *Astrophys. J.* **815** (2015) L25.

- [129] M. Ahlers, Y. Bai, V. Barger, R. Lu, Galactic neutrinos in the TeV to PeV range, *Phys. Rev. D* 93 (2016) 013009.
- [130] S. R. Kelner, F. A. Aharonian, V. V. Bugayov, Energy spectra of gamma-rays, electrons and neutrinos produced at proton-proton interactions in the very high energy regime, *Phys. Rev. D* 74 (2006) 034018. [Erratum: *Phys. Rev. D* 79,039901(2009)].
- [131] M. M. Block, F. Halzen, Experimental Confirmation that the Proton is Asymptotically a Black Disk, *Phys. Rev. Lett.* 107 (2011) 212002.
- [132] T. K. Gaisser, Atmospheric leptons, *EPJ Web Conf.* 52 (2013) 09004.
- [133] G. L. Case, D. Bhattacharya, A new sigma-d relation and its application to the galactic supernova remnant distribution, *Astrophys. J.* 504 (1998) 761.
- [134] M. Ahlers, K. Murase, Probing the Galactic Origin of the IceCube Excess with Gamma-Rays, *Phys. Rev. D* 90 (2014) 023010.
- [135] J. C. Joshi, W. Winter, N. Gupta, How Many of the Observed Neutrino Events Can Be Described by Cosmic Ray Interactions in the Milky Way?, *Mon. Not. Roy. Astron. Soc.* 439 (2014) 3414–3419. [Erratum: *Mon. Not. Roy. Astron. Soc.* 446,no.1,892(2014)].
- [136] M. Kachelrieß, S. Ostapchenko, Neutrino yield from Galactic cosmic rays, *Phys. Rev. D* 90 (2014) 083002.
- [137] F. Effenberger, H. Fichtner, K. Scherer, I. Busching, Anisotropic diffusion of galactic cosmic ray protons and their steady-state azimuthal distribution, *Astron. Astrophys.* 547 (2012) A120.
- [138] D. Gaggero, L. Maccione, G. Di Bernardo, C. Evoli, D. Grasso, Three-Dimensional Model of Cosmic-Ray Lepton Propagation Reproduces Data from the Alpha Magnetic Spectrometer on the International Space Station, *Phys. Rev. Lett.* 111 (2013) 021102.
- [139] M. Werner, R. Kissmann, A. W. Strong, O. Reimer, Spiral Arms as Cosmic Ray Source Distributions, *Astropart. Phys.* 64 (2015) 18–33.

- [140] A. Neronov, D. V. Semikoz, C. Tchernin, PeV neutrinos from interactions of cosmic rays with the interstellar medium in the Galaxy, *Phys. Rev. D* **89** (2014) 103002.
- [141] A. Neronov, D. V. Semikoz, Evidence the Galactic contribution to the IceCube astrophysical neutrino flux, *Astropart. Phys.* **75** (2016) 60–63.
- [142] S. Casanova, B. L. Dingus, Constraints on the TeV source population and its contribution to the galactic diffuse TeV emission, *Astropart. Phys.* **29** (2008) 63–69.
- [143] J. M. Blondin, E. B. Wright, K. J. Borkowski, S. P. Reynolds, Transition to the Radiative Phase in Supernova Remnants, *Astrophys. J.* **500** (1998) 342–354.
- [144] D. B. Fox, K. Kashiyama, P. Mészáros, Sub-PeV Neutrinos from TeV Unidentified Sources in the Galaxy, *Astrophys. J.* **774** (2013) 74.
- [145] M. Mandelartz, J. Becker Tjus, Prediction of the diffuse neutrino flux from cosmic ray interactions near supernova remnants, *Astropart. Phys.* **65** (2015) 80–100.
- [146] D. R. Lorimer, et al., The Parkes multibeam pulsar survey: VI. Discovery and timing of 142 pulsars and a Galactic population analysis, *Mon. Not. Roy. Astron. Soc.* **372** (2006) 777–800.
- [147] M. G. Aartsen, et al., Measurement of the cosmic ray energy spectrum with IceTop-73, *Phys. Rev. D* **88** (2013) 042004.
- [148] M. G. Aartsen, et al., Characterization of the Atmospheric Muon Flux in IceCube, *Astropart. Phys.* **78** (2016) 1–27.
- [149] R. Abbasi, et al., Lateral Distribution of Muons in IceCube Cosmic Ray Events, *Phys. Rev. D* **87** (2013) 012005.
- [150] M. Amenomori, et al., The All-particle spectrum of primary cosmic rays in the wide energy range from  $10^{14}$  eV to  $10^{17}$  eV observed with the Tibet-III air-shower array, *Astrophys. J.* **678** (2008) 1165–1179.
- [151] G. Di Sciascio, Measurement of the Cosmic Ray Energy Spectrum with ARGO-YBJ, *Frascati Phys. Ser.* **58** (2014) 215 (arXiv:1408.6739).



- [152] W. D. Apel, et al., The KASCADE-Grande energy spectrum of cosmic rays and the role of hadronic interaction models, *Adv. Space Res.* 53 (2014) 1456–1469.
- [153] V. V. Prosin, et al., Tunka-133: Results of 3 year operation, *Nucl. Instrum. Meth.* A756 (2014) 94–101.
- [154] R. U. Abbasi, et al., First observation of the Greisen-Zatsepin-Kuzmin suppression, *Phys. Rev. Lett.* 100 (2008) 101101.
- [155] T. Abu-Zayyad, et al., The Energy Spectrum of Ultra-High-Energy Cosmic Rays Measured by the Telescope Array FADC Fluorescence Detectors in Monocular Mode, *Astropart. Phys.* 48 (2013) 16–24.
- [156] The Pierre Auger Observatory: Contributions to the 34th International Cosmic Ray Conference (ICRC 2015), arXiv:1509.03732, in: *Proceedings, 34th International Cosmic Ray Conference (ICRC 2015): The Hague, The Netherlands, July 30-August 6, 2015.*
- [157] K. Rawlins, Cosmic ray spectrum and composition from three years of IceTop and IceCube, *J. Phys. Conf. Ser.* 718 (2016) 052033.
- [158] R. Bellotti, et al., Simultaneous Observation of Extensive Air Showers and Deep Underground Muons at the Gran Sasso Laboratory, *Phys. Rev.* D42 (1990) 1396–1403.
- [159] J. Ahrens, et al., Measurement of the cosmic ray composition at the knee with the SPASE-2/AMANDA-B10 detectors, *Astropart. Phys.* 21 (2004) 565–581.
- [160] B. Peters, Primary cosmic radiation and extensive air showers, *Nuovo Cimento* XXII (1961) 800–819.
- [161] K.-H. Kampert, M. Unger, Measurements of the Cosmic Ray Composition with Air Shower Experiments, *Astropart. Phys.* 35 (2012) 660–678.
- [162] T. K. Gaisser, Primary spectrum and composition with IceCube/IceTop, in: *Cosmic Ray International Seminar: The status and the future of the UHE Cosmic Ray Physics in the post LHC era (CRIS 2015) Gallipoli, Italy, September 14-16, 2015 (arXiv:1601.06670).*

- [163] H. P. Dembinski, J. Gonzalez, Surface muons in IceTop, PoS ICRC2015 (2016) 267.
- [164] A. Aab, et al., Muons in air showers at the Pierre Auger Observatory: Mean number in highly inclined events, Phys. Rev. D91 (2015) 032003. [Erratum: Phys. Rev.D91,no.5,059901(2015)].
- [165] A. Aab, et al., Testing Hadronic Interactions at Ultrahigh Energies with Air Showers Measured by the Pierre Auger Observatory, Phys. Rev. Lett. 117 (2016) 192001.
- [166] M. G. Aartsen, et al., Search for Galactic PeV Gamma Rays with the IceCube Neutrino Observatory, Phys. Rev. D87 (2013) 062002.
- [167] M. G. Aartsen, et al., Search for Sources of High Energy Neutrons with Four Years of Data from the IceTop Detector, Astrophys. J. 830 (2016) 129.
- [168] K. Nagashima, K. Fujimoto, R. M. Jacklyn, Galactic and heliotail-in anisotropies of cosmic rays as the origin of sidereal daily variation in the energy region  $<10^4$  GeV, J. Geophys. Res. 103 (1998) 17429–17440.
- [169] D. L. Hall, et al., Gaussian analysis of two hemisphere observations of galactic cosmic ray sidereal anisotropies, J. Geophys. Res. 104 (1999) 6737–6750.
- [170] B. Bartoli, et al., Medium scale anisotropy in the TeV cosmic ray flux observed by ARGO-YBJ, Phys. Rev. D 88 (2013) 082001.
- [171] R. Abbasi, et al., Measurement of the Anisotropy of Cosmic-ray Arrival Directions with IceCube, Astrophys. J. Lett. 718 (2010) L194–L198.
- [172] R. Abbasi, et al., Observation of Anisotropy in the Arrival Directions of Galactic Cosmic Rays at Multiple Angular Scales with IceCube, Astrophys. J. 740 (2011) 16.
- [173] M. Aartsen, et al., Observation of Cosmic-Ray Anisotropy with the IceTop Air Shower Array, Astrophys. J. 765 (2013) 55.
- [174] M. G. Aartsen, et al., Anisotropy in Cosmic-ray Arrival Directions in the Southern Hemisphere Based on Six Years of Data From the IceCube Detector, Astrophys. J. 826 (2016) 220.

- [175] M. Aglietta, et al., Evolution of the Cosmic-Ray Anisotropy Above  $10^{14}$  eV, *Astrophys. J. Lett.* 692 (2009) L130–L133.
- [176] R. Abbasi, et al., Observation of Anisotropy in the Galactic Cosmic-Ray Arrival Directions at 400 TeV with IceCube, *Astrophys. J.* 746 (2012) 33.
- [177] A. Abeyssekara, et al., Observation of Small-scale Anisotropy in the Arrival Direction Distribution of TeV Cosmic Rays with HAWC, *Astrophys. J.* 796 (2014) 108.
- [178] M. Amenomori, et al., Implication of the sidereal anisotropy of  $\sim 5$  TeV cosmic ray intensity observed with the Tibet III air shower array, *American Institute of Physics Conference Series* 932 (2007) 283.
- [179] A. Abdo, et al., Discovery of Localized Regions of Excess 10-TeV Cosmic Rays, *Phys. Rev. Lett.* 101 (2008) 221101.
- [180] S. Tilav, et al., Atmospheric Variations as observed by IceCube (arXiv:1001.0776), *Proc. 31st Int. Cosmic Ray Conference*, Lodz, Poland (2010).
- [181] P. Desiati, Seasonal Variations of High Energy Cosmic Ray Muons Observed by the IceCube Observatory as a Probe of Kaon/Pion Ratio, *Proc. 32nd Int. Cosmic Ray Conference*, Beijing, China 1 (2011) 78 (arXiv:1111.2735).
- [182] M. Aartsen, et al., Seasonal variation of the muon multiplicity in cosmic rays at South Pole (Paper 0763, arXiv:1309.7006v2), *Proc. 33rd Int. Cosmic Ray Conference*, Rio de Janeiro, Brasil (2013).
- [183] M. Ahlers, P. Mertsch, Origin of Small-Scale Anisotropies in Galactic Cosmic Rays, *Progress in Particle and Nuclear Physics* (2016) in preparation.
- [184] P. Abreu, et al., Search for first harmonic modulation in the right ascension distribution of cosmic rays detected at the Pierre Auger Observatory, *Astropart. Phys.* 34 (2011) 627–639.
- [185] A. Chiavassa, et al., A study of the first harmonic of the large scale anisotropies with the KASCADE-Grande experiment, *PoS ICRC2015* (2016) 281.

- [186] M. Aartsen, et al., Study of the time-dependence of the cosmic-ray anisotropy with IceCube and AMANDA (Paper 0411, arXiv:1309.7006v2), Proc. 33rd Int. Cosmic Ray Conference, Rio de Janeiro, Brasil (2013).
- [187] L. G. Sveshnikova, O. N. Strelnikova, V. S. Ptuskin, Spectrum and anisotropy of cosmic rays at TeV-PeV-energies and contribution of nearby sources, *Astropart. Phys.* 50 (2013) 33–46.
- [188] P. Blasi, E. Amato, Diffusive propagation of cosmic rays from supernova remnants in the Galaxy. II: anisotropy, *JCAP* 1 (2012) 11.
- [189] V. Ptuskin, Propagation of galactic cosmic rays, *Astropart. Phys.* 39 (2012) 44–51.
- [190] M. Pohl, D. Eichler, Understanding TeV-band Cosmic-Ray Anisotropy, *Astrophys. J.* 766 (2013) 4.
- [191] A. D. Erlykin, A. W. Wolfendale, The anisotropy of galactic cosmic rays as a product of stochastic supernova explosions, *Astropart. Phys.* 25 (2006) 183–194.
- [192] R. Kumar, D. Eichler, Large-scale Anisotropy of TeV-band Cosmic Rays, *Astrophys. J.* 785 (2014) 129.
- [193] P. Mertsch, S. Funk, Solution to the Cosmic Ray Anisotropy Problem, *Phys. Rev. Lett.* 114 (2015) 021101.
- [194] G. Giacinti, G. Sigl, Local Magnetic Turbulence and TeV-PeV Cosmic Ray Anisotropies, *Phys. Rev. Lett.* 109 (2012) 071101.
- [195] P. L. Biermann, et al., Cosmic-Ray Transport and Anisotropies, *Astrophys. J.* 768 (2013) 124.
- [196] M. Ahlers, Anomalous Anisotropies of Cosmic Rays from Turbulent Magnetic Fields, *Phys. Rev. Lett.* 112 (2014) 021101.
- [197] M. Ahlers, P. Mertsch, Small-Scale Anisotropies of Cosmic Rays from Relative Diffusion, *Astrophys. J. Lett.* 815 (2015) L2.

- [198] V. López-Barquero, R. Farber, S. Xu, P. Desiati, A. Lazarian, Cosmic Ray Small Scale Anisotropies and Local Turbulent Magnetic Fields, *Astrophys. J.* 830 (2016) 19.
- [199] J. P. Harding, C. L. Fryer, S. Mendel, Explaining TeV Cosmic-Ray Anisotropies with Non-Diffusive Cosmic-Ray Propagation, *Astrophys. J.* 822 (2016) 102.
- [200] K. Scherer, R. D. Strauss, S. E. S. Ferreira, H. Fichtner, Comic ray flux anisotropies caused by astrospheres, *Astropart. Phys.* 82 (2016) 93–98.
- [201] M. Ahlers, Deciphering the Dipole Anisotropy of Galactic Cosmic Rays, *Phys. Rev. Lett.* 117 (2016) 151103.
- [202] M. Ahlers, et al., A New Maximum-Likelihood Technique for Reconstructing Cosmic-Ray Anisotropy at All Angular Scales, *Astrophys. J.* 823 (2016) 10.
- [203] P. Desiati, A. Lazarian, Anisotropy of TeV Cosmic Rays and Outer Heliospheric Boundaries, *Astrophys. J.* 762 (2013) 44.
- [204] N. A. Schwadron, et al., Global Anisotropies in TeV Cosmic Rays Related to the Sun’s Local Galactic Environment from IBEX, *Science* 343 (2014) 988–990.
- [205] M. Zhang, P. Zuo, N. Pogorelov, Heliospheric Influence on the Anisotropy of TeV Cosmic Rays, *Astrophys. J.* 790 (2014) 5.
- [206] V. López-Barquero, et al., TeV Cosmic-Ray Anisotropy from the Magnetic Field at the Heliospheric Boundary, *arXiv eprints* (2016) astro-ph/1610.03097.
- [207] A. Lazarian, P. Desiati, Magnetic Reconnection as the Cause of Cosmic Ray Excess from the Heliospheric Tail, *Astrophys. J.* 722 (2010) 188–196.
- [208] P. Desiati, A. Lazarian, Cosmic rays and stochastic magnetic reconnection in the heliotail, *Nonlinear Processes in Geophysics* 19 (2012) 351–364.

- [209] M. G. Aartsen, et al., IceCube-Gen2: A Vision for the Future of Neutrino Astronomy in Antarctica, arXiv eprints (2014) astro-ph/1412.5106.